Evidence that interglomerular inhibition generates non-monotonic concentration-response relationships in mitral/tufted glomeruli in the mouse olfactory bulb

Authors: Lee Min Leong[1*], David Wharton[4*], Narayan Subramanian[1], Bhargav Karamched[2,3,4], Richard Bertram[2,3,4], Douglas A. Storace[1,2,3]
[1]Department of Biological Science, Florida State University, Tallahassee, FL
[2]Program in Neuroscience, Florida State University, Tallahassee, FL
[3]Institute of Molecular Biophysics, Florida State University, Tallahassee, FL
[4]Department of Mathematics, Florida State University, Tallahassee, FL
***** These authors contributed equally to this work

Communicating Author:
Douglas A. Storace
107 Chieftan Way
Biomedical Research Facility
Department of Biological Science
Program in Neuroscience
Florida State University
Tallahassee, FL 32306
dstorace@fsu.edu

ORCID Numbers:
(L. Leong) = https://orcid.org/0009-0005-2169-0084
(D. Wharton) = https://orcid.org/0009-0000-5365-0056
(R. Bertram) = http://orcid.org/0000-0001-8577-2592
(B. Karamched) = https://orcid.org/0000-0002-6926-7593
(D. Storace) = https://orcid.org/0000-0002-3535-5472

Acknowledgements: This work was supported by funding from NIDCD R01 DC020519.

Conflict of interest: The authors declare no competing financial interests.

Highlights

- We built a model of the olfactory bulb incorporating feed-forward and lateral inhibition.
- Five model predictions were tested using dual-color 2-photon *in vivo* Ca^{2+} imaging.
- The magnitude of MTC suppression scaled with increasing excitation.
- Non-monotonic MTC glomeruli are common and receive input from high affinity ORNs.

Summary. The role of intra- and interglomerular networks in the olfactory bulb (OB) in transforming olfactory receptor neuron (ORN) input across concentration changes remains poorly understood. We addressed this question by implementing a mathematical model of the OB input-output transformation in which the output of each glomerulus is a function of its ORN input, local and lateral inhibition. The model produced outputs with concentration-response relationships that depended on the input ORN Hill coefficient and half-activation value. Some glomeruli responded with monotonic increases or decreases, while others responded with non-monotonic decreases then increases or increased then decreased. The model yielded several novel predictions that challenged recent findings in the field, including the existence of an abundance of non-monotonic responses and that inhibition across the interglomerular network should increase with excitation. We tested these predictions using single and dual-color *in vivo* 2-photon Ca^{2+} imaging from ORN and MTC glomeruli in awake mice. MTC glomeruli responded to odors with monotonic and non-monotonic concentration-response relationships in an odor-specific manner. Notably the mean excitation and suppression across the glomerular population were significantly correlated with one another and half of the MTC glomeruli exhibited some degree of non-monotonicity. The magnitude of non-monotonicity in MTC glomeruli was significantly correlated with the affinity of its ORN input and decreasing MTC glomeruli were innervated by low affinity or non-responsive ORN input. The results support a model in which rising levels of local and lateral inhibition will generate heterogeneous concentration-response relationships, which we propose will facilitate odor discrimination.

Introduction.

One of the goals of neuroscience is to define the underlying neural circuits and computations involved in transforming sensory signals into behaviorally relevant information[1-3]. For example, odor recognition must be initiated by the binding of an odor ligand to olfactory receptor neurons (ORNs), each of which express one kind of olfactory receptor (OR) protein (out of ~1000) and have a distinct affinity for each odor[4-9]. Odors evoke varying degrees of activity across the receptor population that must be related to perception. However, low concentrations of an odor will activate high affinity receptors, while higher concentrations of the same odor will saturate those high affinity receptors and recruit low affinity receptor types[10-13]. Consequently, there is a confound between how the identity and concentration of an odor are encoded at the level of ORNs. Without further processing odors would be perceived differently when they are experienced at different concentrations or in the presence of other background odor stimuli.

Each ORN type maps to the olfactory bulb (OB) in OR specific channels called glomeruli[4,5]. Mitral and tufted cells (MTCs) extend their apical dendrite into a single glomerulus and project their axons to the rest of the brain[14-16]. Therefore, each glomerulus contains the input-output transformation for a given olfactory receptor, which can be influenced by a complex synaptic network that includes inhibitory interneurons[17-20]. The inhibition provided by interneurons is an important element of the neural processing of ORN input and comes in two forms. One involves feed-forward inhibition where high-sensitivity inhibitory interneurons are excited by ORN input and actively inhibit MTCs[17,21,22]. A second process involves normalization in which MTC output reflects a combination of its afferent input, as well as the collective activity across a population[23-25]. Both processes are thought to be important in performing sensory transformations that may be important in expanding the dynamic range of ORN inputs, enhancing contrast across glomeruli, decorrelation and normalization[18,26,27].

The role of the two kinds of inhibition on transforming different ORN inputs across concentration changes remains poorly understood. The OB contains an inhibitory interglomerular network in which increasing excitatory input drives inhibition across the OB[12,28]. Because ORNs have relatively narrow dynamic ranges, interglomerular networks should in principle generate monotonic and non-monotonic concentration response relationships[9,28-36]. However, imaging experiments from MTC glomeruli, and models of different kinds of interglomerular networks have revealed primarily monotonic concentration-response relationships[11,12,37-39].

We investigated the role of feed-forward and lateral inhibition in the OB by implementing a mathematical model in which ORN inputs are transformed by intraglomerular feed-forward inhibition and interglomerular normalization. The model predicted the existence of categories of monotonic and non-monotonic concentration-response relationships that depended on the ORN parameters. Non-monotonic and monotonically decreasing responses depended on rising levels of inhibition, and originated primarily from high and low affinity ORN inputs, respectively.

We tested these predictions using single and dual-color *in vivo* 2-photon Ca^{2+} imaging from ORN and MTC glomeruli in awake mice across a large concentration range. MTC glomeruli within the same field of view responded with both monotonic and non-monotonic concentration-response relationships that were odor-specific and closely approximated those generated by the model.

Increasing odor concentration increased the mean response of glomeruli that were excited and suppressed by the odor, consistent with the presence of rising levels of inhibition. Notably, nearly half of the MTC glomeruli responded with non-monotonic concentration-response relationships, and the degree of non-monotonicity for MTC glomeruli was significantly correlated with its corresponding ORN affinity. Finally, exclusively suppressed glomeruli typically originated from low affinity or non-responsive ORNs.

Our observations that the magnitude of MTC suppression increases with excitation, and that non-monotonic concentration-response relationships are common challenges recent findings in the field. Additionally, we demonstrate that a mathematical model that incorporates both intraglomerular feed-forward inhibition and global interglomerular inhibitory connectivity generates predictions that closely approximate *in vivo* measurements from ORN and MTC glomeruli. In the model and in the data, increases in concentration evoke higher levels of excitation across the glomerular population, which causes an increase in the magnitude of inhibition and suppression of many non-stimulated glomeruli. High affinity ORNs will saturate in response to higher concentrations and will be susceptible to the influence of local and interglomerular inhibitory processes. Therefore, the OB input-output transformation of each glomerulus is shaped by the balance of its input excitation and rising inhibition, and that non-monotonic MTC concentration-response relationships are widespread and the natural consequence of ORNs with a small dynamic range and intra- and interglomerular inhibition. We propose that heterogeneous concentration-response relationships will facilitate odor discrimination.

Methods.

A subset of these data were included in a previous publication that analyzed adapting properties of MTC odor responses[40].

Mathematical Modeling.

The model is based on ideas described in [17] and incorporates two forms of inhibition: local and lateral. The output of the ORNs is dependent upon the odorant concentration, [odorant], and is described mathematically by the sigmoidal Hill function:

$$\text{ORN} = \frac{\upsilon\,[\text{odorant}]^n}{\kappa^n + [\text{odorant}]^n} \tag{1}$$

All variables and parameters are dimensionless, and [odorant] ranges from 0 to 1. The parameter υ sets the maximum value of ORN and is assumed to be the same for all ORNs. The other two parameters are the half-activation constant, κ, and the Hill coefficient, n, which sets the steepness of the ORN's response (higher values of n yield steeper response functions). To generate a large ($N = 949$) heterogeneous population of ORNs, N combinations of parameter values were sampled from a uniform distribution on the intervals of (0,2) for κ and (1,4) for n. The ORN signal is then subject to presynaptic inhibition from other glomeruli before entering the target glomerulus, producing a "normalized ORN" value $\overline{ORN}$:

$$\overline{\text{ORN}} = \frac{\text{ORN}}{1+\mu} \tag{2}$$

where $\mu = \sum_{i=1}^{N} \text{ORN}_i / N$ is the average value of all ORN activity. This normalized output of the ORN is then the input to periglomerular and MTCs, reflected in the variables PG and MTI, respectively. The circuitry involved in this lateral inhibition is not specified in the model, and could reflect the action of short axon cells onto external tufted cells, which then serve as input to MTCs and PG cells, as previously described[26,28]. The PG and MTI variables are described with increasing Hill functions:

$$\text{PG} = \frac{\beta\, \overline{\text{ORN}}^{4.5}}{\kappa_p^{4.5} + \overline{\text{ORN}}^{4.5}} \tag{3}$$

$$\text{MTI} = \frac{\overline{\text{ORN}}^{3}}{\kappa_m^{3} + \overline{\text{ORN}}^{3}} \tag{4}$$

where β, κ_p, and κ_m are parameters that are assumed to be the same for each PG and MTI. They are set so that PG begins to activate at lower values of $\overline{\text{ORN}}$ than MTI and saturates at a lower value (saturation value of β) than MTI (saturation value of 1). The higher affinity of PG cells is a key element of the half-hat coding hypothesized by Cleland[17,18]. The output of each glomerulus, MTC output, is then the difference between MTI and the inhibition from PG cells,

$$\text{MTC output} = \text{MTI-PG} \tag{5}$$

Parameter values are given in **Table 1**.

Symbol	Value(s)	Description
[odorant]	[0,1]	concentration of input stimuli
v	2	Maximum ORN value
n	random(1,4)	ORN Hill coefficient
κ	random(0,2)	ORN half-activation value
β	0.6	Maximum PG value
κ_p	0.5	PG half-activation value
κ_m	1	MTI half-activation value

Table 1: Parameter values used in model simulations

Transgenic mice.

GCaMP6f was targeted to MTC glomeruli by mating the Ai148 GCaMP6f transgenic reporter line (Jax stock #030328) to the Tbx21-cre transgenic line (Jax stock #024507)[40-42]. GCaMP6s was targeted to olfactory receptor neuron (ORN) glomeruli by mating the tetO-GCaMP6s transgenic reporter line (Jax stock #024742) to the OMP-tTA transgenic line (Jax stock #017754)[40,43]. This OMP-tTA-tetO-GCaMP6s line was mated with the Tbx21-cre transgenic line (Jax stock #024507) to create a triple transgenic line (OMP-tTA-tetO-GCaMP6s Tbx21-cre) expressing GCaMP6s in the ORN

glomeruli and allowing for cre-dependent expression in the MTC glomeruli. GCaMP8m was targeted to MTC glomeruli by mating the TIGRE2-jGCaMP8m-IRES-tTA2-WPRE transgenic reporter line (Jax stock # 037718) to the Tbx21-cre transgenic line (Jax stock #024507)[40-42]. Genotyping was performed by Transnetyx (Cordova, TN) and male and female adult offspring that expressed eGFP and Cre recombinase for MTC glomeruli or eGFP, tTA and Cre recombinase for ORN glomeruli were used for experiments. We further confirmed that the fluorescent proteins were expressed in the excepted cell population in histological samples (described under Histology).

Surgical procedures.

All procedures were approved by the Florida State University Animal Care and Use Committee. Male and female adult (> 21 days) transgenic mice were anesthetized using ketamine/xylazine (90 / 10 mg/kg, Zoetis, Kalamazoo, MI), placed on a heating pad and had ophthalmic ointment applied to their eyes. Mice were given a pre-operative dose of carprofen (20 mg/kg, Zoetis, Kalamazoo, MI), atropine (0.2 mg/kg, Covetrus, Dublin, OH), dexamethasone (4 mg/kg, Bimeda, La Sueur, MN), and bupivacaine (1.5 mg/kg, Hospira, Lake Forest, IL). Fur was removed from the top of the skull using a depilatory agent and rinsed, after which the skin was scrubbed with 70% isopropyl alcohol and iodine (Covidien, Mansfield, MA). An incision was made to remove the skin over the skull and blunt dissection was used to remove the underlying membrane. Dental cement (Metabond, Covetrus, Dublin, OH) was used to attach a custom headpost to the skull, which was held using a custom headpost holder. After the cement finished drying, the bone above the OB was either thinned using a dental drill (Osada, XL-230, Los Angeles, CA) and covered with cyanoacrylate to improve optical clarity or was removed and replaced with cover glass.

For the dual color input-output experiments, stereotaxic injections were carried out immediately after the craniotomy. 500 nl of AAV1. Syn.Flex.NES-jRCaMP1b.WPRE.SV40 (Addgene, 100850-AAV1, Watertown, MA) was injected into the right olfactory bulb of OMP-tTA-tetO-GCaMP6s Tbx21-cre triple transgenic mice before sealing the cranial window with a #1 cover glass. Upon completion of the surgery, the mouse was allowed to recover on a heating pad until they were fully ambulatory. Animals were given a post-operative dose of carprofen at the end of the day of surgery and for at least 3 days post-operatively. The AAV was allowed to express for at least two weeks before beginning imaging experiments.

Histology.

We validated the targeting of the optical sensors used in this study based on endogenous fluorescence expression of GCaMP6f (MTCs), GCaMP6s (ORNs), GCaMP8m (MTCs) and jRCaMP1b (MTCs) in histological samples observed using an appropriate filter set on either a Zeiss Axioskop epifluorescence microscope or a Nikon CSU-W1 spinning disk confocal microscope. Mice were euthanized (euthasol) following imaging and either underwent cardiac perfusion with phosphate buffered saline and 4% paraformaldehyde or had their brains directly extracted and post-fixed in 4% paraformaldehyde before being cut on a vibratome in 40 µm sections (Leica VT1000S, Deer Park, IL). OB sections were mounted on slides and were coverslipped using Fluoromount-G containing DAPI (SouthernBiotech, Birmingham, AL).

2-photon imaging.

Imaging was performed using a Sutter MOM 2-photon microscope equipped with an 8 kHz (30.9 Hz) resonant scanner (Cambridge Technology, USA) and an emission pathway equipped with a GaAsP PMT (#H10770PA-40-04, Hamamatsu, Japan). Laser excitation was provided using either an Alcor 920-2W laser (920 nm for GCaMP imaging) with power modulated by an internal acousto-optic modulator or a Spectra-Physics DS+ between 940-980 nm for GCaMP imaging or 1100 nm for jRCaMP1b imaging, with power modulated by a Pockels cell (Model #350-105-02, Conoptics, Danbury, CT). Imaging was performed using a Nikon 16x 0.8 N.A. or a 10x 0.5 N.A. objective lens[44]. Laser power was confirmed to be less than 150 mW at the output of the objective lens measured using a power meter (Newport 843-R) for scanning areas ranging between 711 μm^2 - 1138 μm^2.

Odorant delivery.

Methyl valerate (99% pure, CAS #624-24-8, Sigma-Aldrich, #148997), isoamyl acetate (99% pure, CAS #123-92-2, Thermo Scientific #150662500), benzaldehyde (> 99.5% purity, CAS #100-52-7, Sigma Aldrich #418099), acetophenone (99% pure, CAS #100-52-7, Fisher Scientific #AAA12727AP), and 2-phenylethanol (> 99% CAS #60-12-8, Sigma-Aldrich #77861) were used at concentrations between 0.05 and 5.5 % of saturated vapor. The olfactometer design involved air being pushed through vials of pure odor using a syringe pump (NE-1000, PumpSystems, Farmingdale, NY) running at different flow rates (0.25 – 28 ml /min)[40]. This odor stream underwent an initial air dilution with a lower flow rate of clean air (30 ml/min). The resulting odorized air stream connected to a dual 3-way solenoid valve (360T041, NResearch, West Caldwell, NJ) which was connected to an exhaust, a clean air stream and a Teflon delivery manifold which served as the final delivery apparatus placed in front of the mouse's nose. The delivery manifold had a higher flow rate of clean air constantly flowing through it (450 ml/min), which provided a second air dilution. At rest, the solenoid sent the odorized air stream to the exhaust, and the clean air stream to the animal; odor delivery occurred by triggering the solenoid which caused the odor to be injected into the delivery manifold.

For the dual color input-output experiments, the odorants methyl valerate, isoamyl acetate, acetophenone, and methyl salicylate (99% pure, CAS#119-36-8, Sigma-Aldrich #M2047) were diluted in mineral oil to 0.002%, 0.008%, 0.046%, 0.278%, 1.667% and 10%. The olfactometer setup uses an air pump that is constantly delivering clean air to two mass flow controllers (MC-100SCCM, and MC-1SLPM, Alicat, Tucson, AZ).

The odor mass flow controller (MC-100SCCM) controls the air flow that passes through the odor vials (50 ml/min for this study), the dilution mass flow controller (MC-1SLPM) provides a higher flow rate of air (450 ml/min for this study) that dilutes the odorized air (i.e., the odors were delivered at 10% saturated vapor). The mass flow controllers are each connected to a 4-valve manifold (360T081, NResearch, West Caldwell, NJ) where the odor vials are connected in between. At any given time, only one of the four pairs of manifold valves open to allow for the odor air stream to blend with the dilution air stream to deliver a particular concentration of the mineral oil diluted odors. The resulting odorized air stream connected to a dual 3-way solenoid valve (360T041, NResearch, West Caldwell, NJ) which was connected to an exhaust, a clean air stream and a Teflon delivery manifold which

served as the final delivery apparatus placed in front of the mouse's nose. The delivery manifold has a separate air pump that delivers clean air at a flow rate that is matched to the flow rate output of the mass flow controllers. The 3-way solenoid valve sends the odorized air stream to the exhaust and the clean air stream to the mouse prior to odor trigger. Triggering the 3-way solenoid causes the odor to be injected into the delivery manifold. The odor delivery time-course for both olfactometer setups were confirmed using a photoionization detector (200C, Aurora Scientific, Aurora, ON)[11,40,45].

Imaging procedures.

Prior to data collection mice were positioned underneath the microscope and the headpost holder angle was adjusted to optimize the imaging field of view. During data collection, awake head-fixed mice were placed underneath the microscope objective with the olfactometer and either a thermocouple (Omega 5TC-TT-K-36-36, Newark) near its nose, or a pressure sensor embedded in the olfactometer to measure respiration. The signals from the respiration sensor were amplified and low-pass filtered using a differential amplifier (Model 3000, AM-Systems, Sequim, WA), which was recorded by the imaging system. For GCaMP6f imaging experiments (**Figures 2-6**), odors were delivered at concentrations between 0.05 – 5.5 % of saturated vapor in trials separated by a minimum of 3 minutes. For glomerular imaging using jGCaMP8m (MTCs), jRCaMP1b (MTCs) and GCaMP6s (ORNs), odors were delivered in 6 concentration steps between 0.002% - 10% of pure odor diluted in mineral oil at 10% of saturated vapor, and air trials in which the odor stream was passed through a previously unused vial. For each animal, we prioritized measuring multiple repetitions for each concentration for a particular odor before a second odor was attempted.

Data analysis.

Frame Subtraction Analysis. The mean fluorescence and frame subtraction images are from the average of at least two single trials (**Figure 2A, 7C**). The mean fluorescence images are generated from the average of all the frames during the imaging trial, or all the frames prior to odor stimulation. The frame subtraction images were generated by subtracting an average of the 19 frames during odor stimulation from the average of 9 frames prior to the stimulus. The resulting image underwent two passes of a low-pass spatial filter, and the fluorescence (F) values were converted to $\Delta F/F$ by dividing the fluorescence value of each pixel by the mean of at least 60 consecutive frames in the image stack in Turbo-SM. The intensity scale range is fixed to the same minimum and maximum range for all concentrations for each odor (**Figure 2**).

Processing and segmentation. Following data acquisition, the raw image files were spatially and temporally averaged from 512x512 pixels sampled at 30.9 Hz to 256x256 pixels sampled at 7.72 Hz. The resulting data were exported to TIFF format for all subsequent analysis. Occasional recordings with motion artifact that made it impossible to interpret the measurements were discarded from subsequent analysis. Glomerular regions of interest were manually segmented in custom software (Turbo-SM, SciMeasure, Decatur, GA) and were identified based on their morphological properties in the mean fluorescence, and functional responses in a frame subtraction. The pixel areas containing the regions of interest were saved and the fluorescence time course values from each region of

interest were extracted for subsequent analysis. Fluorescence time course values were converted to ΔF/F by dividing each trace by the mean of the frames prior to odor stimulation. Odor response amplitudes and corresponding Z-Scores were calculated as the largest difference between a 1200 msec window during the odor presentation and the time prior to odor stimulation.

Other analyses. Population descriptive statistics were quantified in responsive glomeruli which were defined as those in which an odor evoked a minimum of a 5 standard deviation change from baseline at any concentration (**Figure 2F**). Threshold and best response are defined as the lowest concentration evoking a response, and the concentration evoking the largest response, respectively (**Figure 2G-H**). For all other analyses, glomeruli were included that responded with a minimum of 3 standard deviations above baseline at some concentration. Population measurements of the different response categories were generated by averaging the fluorescence time course from all the glomeruli in a field of view assigned to that category (**Figure 3E-F**).

For the spatial maps of glomerular ΔF/F and categorical responses, glomeruli that did not respond at any concentration are indicated using cross-hatching (**Figure 4A-B**). For responsive glomeruli, concentrations that evoked a change of less than 2 standard deviations were assigned a value of zero to facilitate visual analysis (**Figure 4A**, *white polygons*). For the network category analysis (**Figure 4B-C**), the response category of each glomerulus was included for preparations that were tested to more than one odor. The network graph in **Figure 4C** was generated by plotting the categories of each glomerulus for different odors using the graph function in MATLAB.

The relationship between excitation and suppression was quantified by averaging the response from all glomeruli that responded to the highest concentration with excitation and suppression, respectively (**Figure 5**). The mean excited and suppressed response for each preparation are plotted together, with the responses from individual preparations connected with a line (**Figure 5E**). The correlation between these values were quantified for individual preparations and across the population using the corrcoef function in MATLAB (**Figure 5D-E**). The variance explained was quantified by binning the mean excitation and suppression value measured for each concentration (**Figure 5E**, black solid line), and fitting them with a sigmoid (**Figure 5E**, black dashed line) [38].

To avoid biasing the proportion of the dataset identified as non-monotonic, we analyzed the GCaMP6f dataset using two approaches. The first approach used the Monotonicity Index (MI), a metric that computes the degree of non-monotonicity in a concentration-response function (**Figure 6**) [46,47]. The MI of individual glomeruli was calculated by computing the d-prime value by measuring the concentration-response function (CRF) in ΔF/F.

$$D' = \frac{CRF + CRF_{max}}{\sqrt{\sigma^2_{max} + \sigma^2}} \tag{6}$$

The CRF_{max} is the response at the concentration with the largest ΔF/F change from the baseline and CRF is the ΔF/F change at each concentration. σ^2_{max} is the response variance at the highest odor concentration, while σ^2 is the response variance at each odor concentration. MI was then computed

as the minimum D' measured at concentrations beyond the one evoking the maximum ΔF/F response. Consequently, a monotonically increasing glomerulus is assigned a value of 0, while glomeruli with non-monotonic concentration response functions are assigned negative values. Glomeruli with moderate non-monotonic shapes are closer to 0, while those with a larger decrease are assigned increasingly negative values. For the analysis in **Figure 6**, MI values were quantified for all glomeruli in the GCaMP6f data set except for exclusively suppressed glomeruli because they are assigned large MI values. The second approach quantified the general slope of the MTC concentration-response function[36]. The linear slope of MTC glomeruli was quantified by first performing a linear interpolation between each consecutive pair of points in the concentration-response relationship. The polyfit function in MATLAB was then used to find the average slope of each line.

half-maximum values were quantified by performing a linear interpolation of the concentration-response relationship for each glomerulus (linearinterp fittype in MATLAB) (**Figures 6-7**, vertical lines). The half-maximum value was defined as the concentration evoking the half-maximum response in the linear interpolation except for the caveat in which glomeruli with a response to the lowest concentration that was greater than the half-maximum were assigned a half-maximum value of 0.05% (e.g., **Figure 6B**, roi9).

Hill equation fits of monotonically increasing glomeruli were performed in glomeruli exhibiting MI values greater than -0.5, Hill fits were calculated using the following equation where *X* is the response (in ΔF/F) of the glomerulus at each concentration, and *k* is the half-saturating value estimated from a linear interpolation of the concentration-response function.

$$\frac{X^n}{X^n + k^n} \tag{7}$$

Fits were only analyzed if they met the following criteria: the Hill coefficient was between 0.75 and 6; the r^2 value was greater than 0.9, the root mean sum of squares was less than 0.1 and the sum of square error was less than 0.1[9].

The trajectory plots were generated by plotting the odor response amplitudes of 3 glomeruli exhibiting exclusively increasing responses, or a combination of all response categories using the plot3 function in MATLAB (**Supplementary Figure S4**).

Results

A model that combines intra- and interglomerular processing predicts four types of concentration-response relationships in MTC glomeruli.

We generated a model to better understand how intra- and interglomerular processing transforms the concentration-response properties of different ORN inputs (see Methods for model equations and parameter values). The output of each glomerulus (**Figure 1A**, d) was a function of its ORN input (**Figure 1A**, a), input from local interneurons that are activated by ORN input and provide inhibition onto the MTC output (**Figure 1A**, b), and inhibitory interglomerular connectivity acting presynaptically to scale down the ORN input (**Figure 1A**, c). ORNs modeled using the Hill equation

served as input both to MTCs and inhibitory PG interneurons whose activation was similarly described by a Hill function, but with the PG response function left-shifted relative to the MTC response function (**Figure 1B**, PG). The difference between these two response functions was then taken as the output from the MTC (**Figure 1B**, MTC output). The MTC output, which is relative to the basal level of activity, has a half-hat shape that shows a dip to negative values for low ORN activation and an increase for higher ORN activation (**Figure 1B**, MTC output).

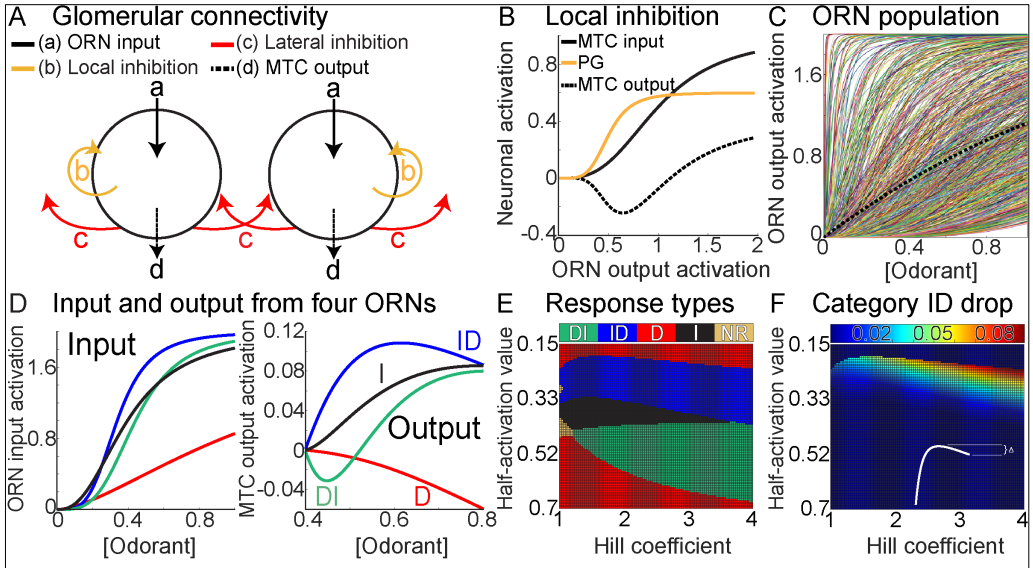

Figure 1: (**A**) Model of the glomerular input-output transformation. (**B**) Local inhibition alone generates a half-hat response in MTCs. (**C**) The population of ORNs in the model (thin lines) used to calculate the normalization function (dashed line). (**D**) The concentration-response relationships of four ORNs (left) and their corresponding MTC output (right) reflecting both local and lateral inhibition. Output responses were categorized based on the shape of the concentration-response relationship: I, increasing; ID, increasing then decreasing; DI, decreasing then increasing; D, decreasing. (**E**) MTC responses for different ORN Hill coefficients and half-activation values. (**F**) The decrease from the maximum to the terminal odorant concentration for combinations of Hill coefficients and half-activation values that result in an ID response.

Interglomerular processing was modeled by generating a population of 949 ORNs with Hill coefficients sampled from a uniform distribution from 1 to 4, consistent with previously published work (**Figure 1C**, thin lines)[9-11,48,49]. Odor affinities (their half-maximum values) were sampled from a uniform distribution on the interval between 0 and 2 (**Figure 1C**). The model is dimensionless, as are the half-maximum values for the receptors. The ORN input to the MTCs and inhibitory PG cells was divided by the mean of the ORN activation function to reflect lateral presynaptic inhibition from all glomeruli (**Figure 1C**, dashed black line).

Four examples of ORN input and corresponding MTC output across a concentration range are illustrated in **Figure 1D** (the colors are matched across the two subpanels). The model output in response to four input functions could be broadly described as having concentration-response relationships that monotonically increased (I), monotonically decreased (D), transitioned from suppressed to excited (DI) or increased to a point at which further concentration increases evoked progressively smaller responses (ID) (**Figure 1D**, right subpanel).

The types of MTC responses are shown with color coding in **Figure 1E** over a grid of values of the ORN Hill coefficient and half-activation constants. The ORNs with the highest affinities had a purely decreasing response to increasing odor concentrations (**Figure 1E**, D, top red regions). In these cases, the MTC output reached its maximum at low odor concentrations and could only decline due to lateral inhibition as other glomeruli became activated at higher concentrations. For ORNs with lower, but still relatively high affinities, the typical response was an initial increase followed by a decrease (**Figure 1E**, ID, blue region). In these cases, strongly activated ORNs near saturation were dominated by increasing lateral inhibition. For lower-affinity ORNs the response was purely

increasing, particularly when the ORN response function was relatively linear (**Figure 1E**, I, black region). At even lower affinities the typical response was a decrease, followed by an increase (**Figure 1E**, DI, green region). In this case, inhibition dominated the MTC output prior to its strong activation at higher odor concentrations, producing a DI response. Finally, at the lowest affinities the response was purely decreasing, reflecting dominance of inhibition over all odor concentrations considered (**Figure 1E**, D, red region).

In principle, D responses can be generated by feed-forward suppression within a range of concentrations (e.g., **Figure 1B**, dashed line between 0 and 0.6), or in the case of spontaneously active ORNs suppressed by interglomerular inhibition. ID responses cannot, however, result from the local inhibition motif used in our model. Instead, they depend upon lateral inhibition, which we hypothesize results from higher levels of interglomerular inhibition resulting from activation of lower affinity ORN glomeruli (**Figure 1C**, dashed black line). We tested this hypothesis by excluding lateral inhibition (normalization) from the model, which resulted in a loss of the ID response types (**Supplementary Figure S1A-B**).

A consequence of this framework is that the magnitude of non-monotonicity should be heterogeneous and originate from higher affinity glomerular input that saturates at lower concentrations. A quantification of the decrease in MTC activation from the maximum over the grid of ORN parameters evoking ID responses revealed a gradient of non-monotonic drops (**Figure 1F**). Most of the parameter values in the grid that produced a large drop in MTC activation following a peak had small ORN half-activation values indicating high affinity for the odor.

The structure of the interglomerular inhibitory network is currently unknown[28,38,50]. The results shown in **Figure 1** were obtained using all-to-all coupling (a clique) among the glomeruli. We also considered the case in which input from 5 and 10 randomly chosen glomeruli provided the interglomerular inhibition, which resulted in different average ORN activation curves used in the normalization of ORN input to glomeruli (Eq. 2) (**Supplementary Figure S1C**). Generally similar response categories were present when performing normalization based on this random subset of ORNs. Importantly, all four types of response patterns were produced using the two different normalization functions (**Supplementary Figure S1D**). It is clear, then, that the four different response types are generic, while the shapes and extent of the regions in the 2-parameter grid that produce the different types of responses depend on the structure of the interglomerular inhibitory network.

In vivo measurements of concentration-response relationships in MTC glomeruli.

We tested these predictions in a data set in which odor responses were measured from MTC glomeruli across a ~100-fold change in concentration using *in vivo* 2-photon Ca^{2+} imaging in awake mice. Imaging was performed in transgenic mice in which GCaMP6f was selectively expressed in MTCs and their corresponding apical dendrites innervating the glomerular layer (**Figure 2A**, *mean fluorescence*). We histologically confirmed targeting of GCaMP6f to MTCs in 3 preparations (*not shown, but see* [40]). Frame subtraction analyses from different preparations illustrate that odors evoked different patterns of excited and suppressed responses within the same field of view (**Figure 2A**, *white versus black regions in frame subtractions*). The specific activation pattern across the

glomerular population was a complex function of odor concentration (**Figure 2A**, *compare over concentration range 0.05 to 5.5%*). Many glomeruli became increasingly excited (monotonically increasing, I) or suppressed (monotonically decreasing, D) at higher concentrations (**Figure 2A**, I vs D). Some glomeruli exhibited nonlinear changes in response to increasing concentration in which they first decreased then increased (DI), while others increased and then decreased (ID) (**Figure 2A**, DI vs ID).

The response from each glomerulus was segmented, and the fluorescence time course and odor response amplitudes (ΔF/F) and corresponding Z-scores were calculated as the largest difference in a 1200 msec moving window between the odor stimulation period and the baseline fluorescence. We quantified the concentration-response relationships in a population of glomerulus-odor pairings that included 736 individual glomeruli in 20 different preparations (36.8 ± 3.3 glomeruli per preparation, ranging from 13-64). At least one odor

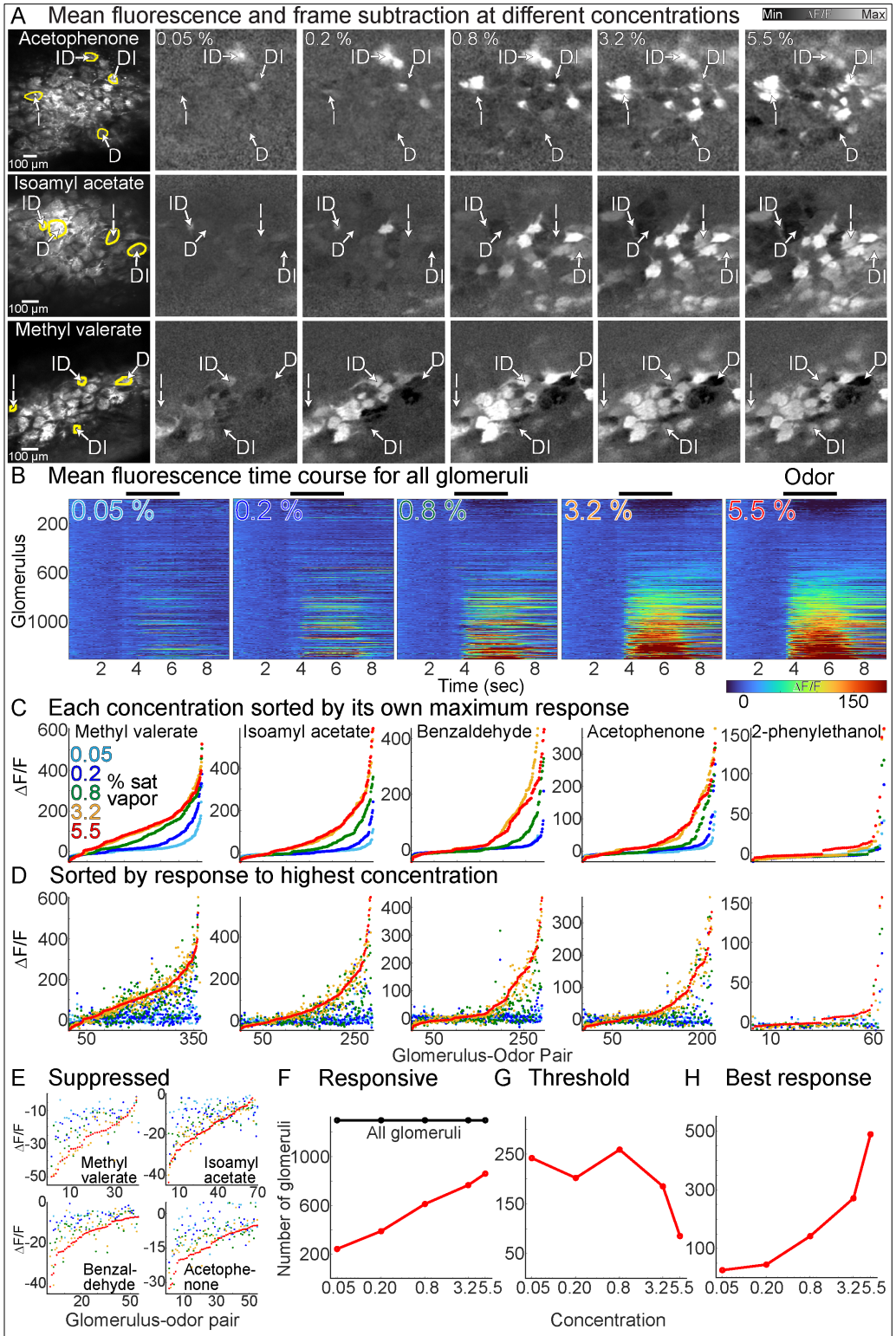

Figure 2: (**A**) Mean fluorescence (left subpanel) and frame subtractions illustrating MTC activation at different concentrations in 3 preparations (rows). The intensity scale is fixed within each preparation. The arrows highlight glomeruli with increasing (I), decreasing (D), increasing-decreasing (ID) and decreasing-increasing (DI) concentration-response relationships. (**B**) Fluorescence time course from all glomerulus-odor pairings. The color scale is fixed across the 5 concentrations. (**C**) Response to all glomeruli for each odor sorted by the maximum response to each concentration (colors). (**D**) Same arrangement as panel **C** except that glomeruli are sorted by the maximum response to the highest concentration. (**E**) Data from panel **D** cropped to visualize suppressed glomeruli. (**F-H**) Descriptive statistics.

was delivered to each preparation at 5 different concentrations, which included the odors methyl valerate (n = 14), isoamyl acetate (n = 7), benzaldehyde (n = 7), acetophenone (n = 5), and 2-phenylethanol (n = 1). The data set includes 6495 glomerulus-odor pairings across all tested odors and concentrations (**Figure 2B**). The fluorescence time course versus amplitude of all glomerulus-odor pairings illustrates that higher concentrations typically evoked stronger degrees of excitation and suppression in more glomeruli (**Figure 2B**), though there are instances where this is not true, as discussed next.

We examined the relationship between concentration and response magnitude at the population level by plotting the ΔF/F evoked for each glomerulus-odor pairing for different odors (**Figure 2C-D**). Sorting glomerular responses from smallest to largest for individual concentrations illustrates that relatively few glomeruli are activated at low concentrations, while the number of activated glomeruli and their overall response amplitude increased at higher concentrations (**Figure 2C**). Sorting glomeruli by their response to the highest concentration more clearly visualizes concentration-response heterogeneity across the population (**Figure 2D**). For many glomeruli, the response to the highest concentration evoked the largest amplitude response (**Figure 2D**, the red point is above the others), although other glomeruli responded with a sub-maximal response to the highest concentration (**Figure 2D**, points of other colors are above red). For glomeruli with suppressed responses, the highest concentration tended to evoke the strongest magnitude of suppression, but not always (**Figure 2E**, data are cropped from panel **D**).

We quantified these observations using a statistical threshold in which significantly responsive glomeruli were defined as responding to the odor with a 5 standard deviation change from the pre-odor frames. The number of significantly responsive glomeruli increased as a function of odor concentration (**Figure 2F**). A similar analysis was used to define the lowest concentration that evoked a significant response for each glomerulus (the “threshold” concentration), and the concentration that evoked the strongest response (the “best” concentration). Of the responsive glomeruli, approximately half had a threshold response of 0.8% of saturated vapor, while the remaining first responded to a lower or higher concentration (**Figure 2G**). About half of the glomeruli responded most strongly to the highest tested concentration, while the remainder responded most strongly to a lower concentration (**Figure 2H**). Increasing or decreasing the statistical threshold altered the number of “responsive” glomeruli in the data set but did not substantially change the mean threshold and best response of the glomeruli (*not shown*).

Examples of different MTC response types.

Representative examples from four different preparation-odor pairings illustrate that monotonic and non-monotonic glomerular concentration-response relationships were consistent across single trials and often present in the same field of view (**Figure 3A-D,** all four glomeruli in each subpanel were simultaneously imaged in the same field of view). Glomeruli categorized as I exhibited continuously rising response amplitudes as a function of concentration, while D glomeruli were more strongly suppressed at higher concentrations (**Figure 3A-D,** 1st two subpanels). Glomeruli consistent with the ID response type were also present where higher concentrations drove increased response amplitudes up to a point at which further increases caused progressively smaller, but still excited

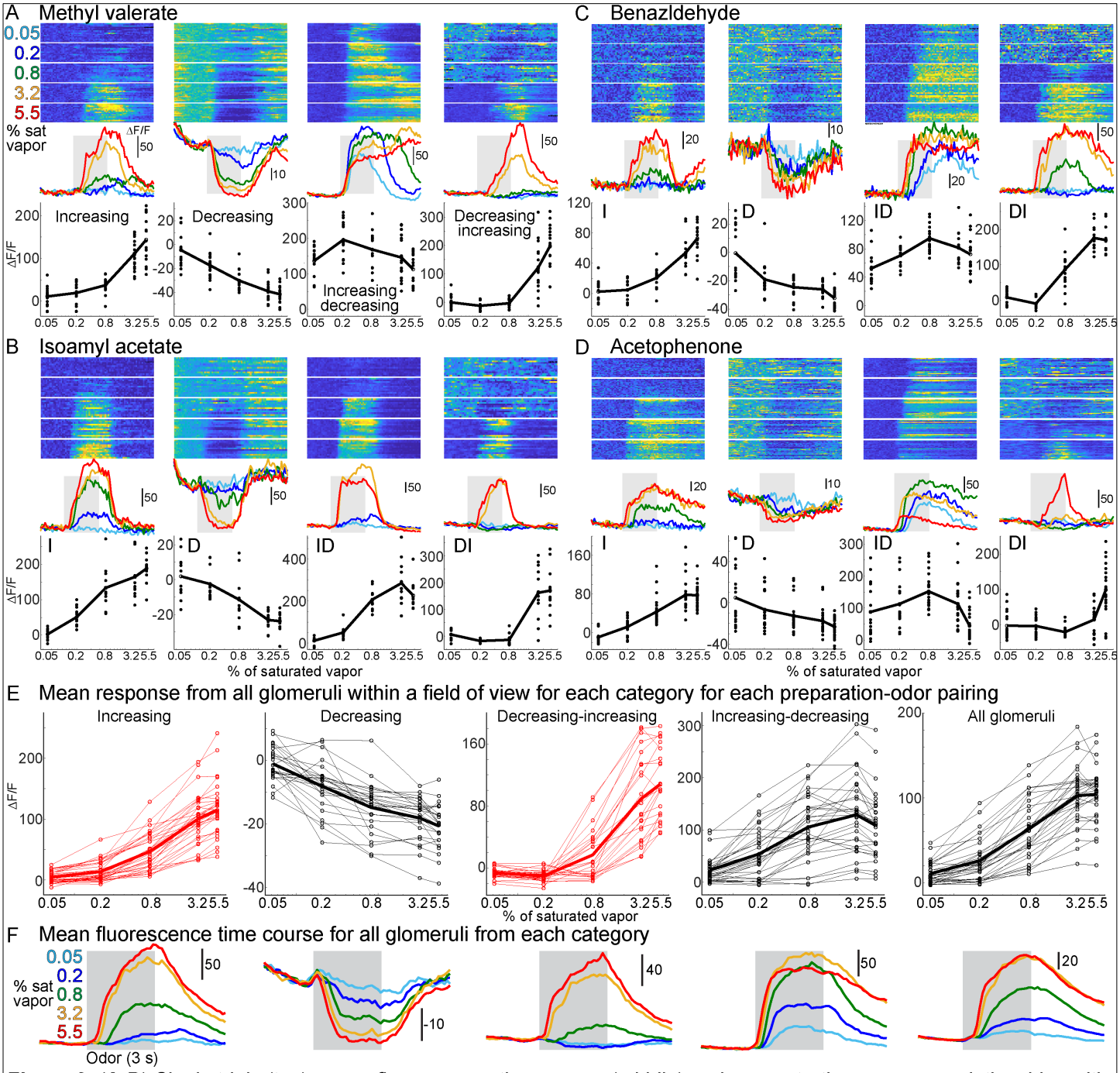

Figure 3: (**A-D**) Single trials (top), mean fluorescence time course (middle) and concentration-response relationships with points indicating the response amplitudes from the single trials for four different preparations. (**E**) Mean concentration-response relationships for each preparation-odor pairing for each response type (1st four subpanels), and across all glomeruli in each field of view (right most subpanel).(**F**) Mean fluorescence time course from all glomeruli in each category.

responses (**Figure 3A-D**, 3rd subpanel). The time course and single trial data for non-monotonic glomeruli highlight the stability of these responses and that the non-monotonic decrease is not a rapid adaptation to the stimulus but instead is a smaller response during the odor presentation[51,52]. Other glomeruli exhibited responses that were characteristic of the DI response type, which were suppressed at a lower concentration, and transitioned to increasingly excited responses at higher concentrations (**Figure 3A-D**, 4th subpanel).

I and D response types were present in 336 and 125 glomeruli, respectively (**Figure 3A-D**). I glomeruli could be well fit with the Hill equation with a mean Hill coefficient of 2.7 ± 0.08 (range of 0.8-5.9, included 190 glomeruli in 16 preparation-odor pairings, the remainder were excluded due to poor

fits, see methods). ID concentration-response relationships were measured in 362 glomeruli. DI responses were present in 92 glomeruli and were suppressed at some concentration but responded to the highest concentration with an increase in fluorescence. Most DI glomeruli were suppressed at 0.2% (42/92) or 0.8% (35/92) of saturated vapor, respectively. Finally, 34 glomeruli exhibited concentration-response relationships that included suppression but could not be clearly fit into any category (e.g., glomeruli that transitioned from strongly excited to suppressed, *not shown*). Thus, of the 915 glomeruli that could be categorized, 37% were of type I, 14% were of type D, 10% were of type DI, and 39% were of type ID.

Plots in which the concentration-response relationship of all glomeruli from each category were averaged together in each preparation-odor pairing illustrate that each response type was consistently present in nearly all preparations (**Figure 3E**, left 4 subpanels, each line represents the average from one preparation). Averaging all responsive glomeruli together within the same field of view demonstrates that higher concentrations drives overall increasing levels of excitation across the glomerular population (**Figure 3E**, All glomeruli, right-most subpanel), although this is often not true at the level of a single glomerulus. The correlation between concentration and mean response was significantly correlated for most individual preparations (0.67 to 0.97, mean of $r = 0.87 \pm 0.08$, $p < 0.05$ in 18/32 preparation-odor pairings). Therefore, excitation scales with concentration in MTC glomeruli.

Different categories of MTC outputs are present when measured with different sensors.

We tested whether the four general concentration-response categories were present in MTC glomeruli measured using two different genetically encoded calcium indicators, jRCaMP1b and jGCaMP8m (**Supplementary Figure S2**). Each response type was consistently present in all four preparations sampled across a large concentration range in 4 different odors (**Supplementary Figure S3A-B,** 2 preparations tested for each sensor). These results suggest that the presence of diverse concentration-response relationships are unlikely to be the consequence of sensor properties specific to GCaMP6f.

Response categories are glomerulus and odor-specific.

Our model indicates that different linear and non-linear MTC concentration-response relationships are due to the specific combination of the Hill coefficient and half-activation value of the corresponding ORNs (**Figure 1E**). One prediction of this is that the response category assigned to each glomerulus should be odor-specific. We tested this in a subset of preparations in which responses were measured to at least 2 different odors (N = 479 glomerulus-odor pairings in 15 preparation-odor pairings in 6 different mouse preparations; between 2-4 odors were tested per preparation). Activity maps ($\Delta F/F$) illustrate that response patterns were concentration-dependent and odor-specific (**Figure 4A**). The different response categories of each glomerulus were identified using the previously described criteria and were mapped using different colors. For each preparation, the same glomerulus could exhibit the same kind of response, or entirely different categorical responses (**Figure 4B**). The effect of odor changes from each category to another is illustrated as a 2-dimensional histogram and a network graph (**Figure 4C-D**). Changing the odor resulted in the same response category in 38.8% of glomeruli, with the most common occurrence being NR glomeruli

remaining as NR (15.6%) (**Figure 4C-D**, NR vs NR). The remainder of the glomeruli transitioned categories, with the most common outcome being that NR transitioned to I (12.5%) (**Figure 4C-D**, NR vs I). Therefore, the proportions of MTC categories observed across the population is a function of odor-driven variability.

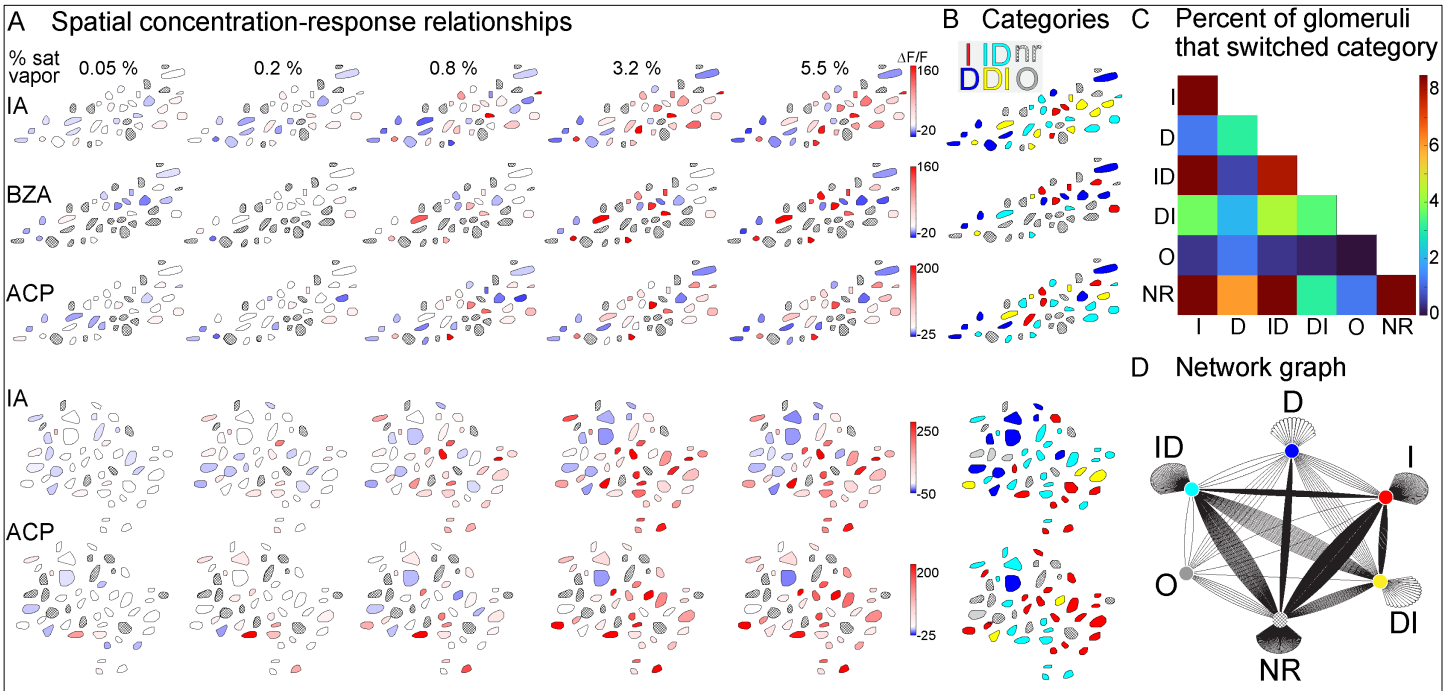

Figure 4: (**A**) Maps of glomerular odor responses (ΔF/F) in different preparations in response to different odors. The colorscale is fixed across all concentrations for each preparation-odor pairing. Glomeruli that do not respond to any concentration are indicated with a hatched overlay. (**B**) Maps of glomerular response categories: I, Increasing, D, Decreasing; DI, Decreasing then increasing; ID, Increasing then decreasing, nr, Non-responsive; O, Other type not clearly associated with any category. IA, isoamyl acetate; BZA, benzaldehyde; ACP, acetophenone; MV, methyl valerate. (**C**) A histogram and network graph illustrate how changing the odor changed the proportions of each response type. (**D**) Network graph illustrating transitions between categories as a function of odor change.

Excitation scales with suppression in MTC glomeruli.

Another prediction from our model is that higher levels of excitation should evoke increasing levels of inhibition (**Figure 1B-C**, *dotted line*). We tested this prediction by comparing the mean of all excited glomeruli within a field of view against the mean of all D glomeruli within a field of view. The response to all concentrations was included for each glomerulus if it responded at any concentration. In four exemplar preparation-odor pairings, there was a strong and sometimes statistically significant relationship between normalized excitation and suppression (**Figure 5A-C,** the number of excited and suppressed glomeruli in each preparation-odor pairing is indicated in panel **B**).

The relationship between excitation and suppression was significantly correlated in 18 out of the 27 preparation-odor pairings included in the analysis (**Figure 5D**, mean r = 0.89 ± 0.01, statistically significant preparations are indicated in red), and when combining all preparation-odor pairings together (**Figure 5E**, r = -0.67, p < 0.001). Additionally, the individual points from all preparations were binned together, the values of which were fit to a sigmoid (**Figure 5E**, thick black line and circles and the dashed line; different fitting parameters yielded similar fits). Although there was variance in the mean values, there was a clear sigmoidal decline which accounted for a

substantial amount of the variance (**Figure 5E**). Therefore, suppression scales with increasing levels of excitation in subsets of MTC glomeruli.

MTC glomeruli ID concentration-response relationships are heterogeneous and have more sensitive odor responses.

Our model predicts that ID responses reflect input from higher affinity ORNs due to receptor saturation, and that differences in the balance of excitation and inhibition should yield differences in the degree of non-monotonicity (**Figure 1D-F**). We quantified the heterogeneity of ID responses using a monotonicity index (MI) which assigns monotonic glomeruli (i.e., I) a value of 0, while non-monotonic glomeruli (e.g., ID) are assigned increasingly negative values depending on the magnitude of the decrease[46,47]. Concentration-response relationships from simultaneously imaged glomeruli in two different preparations illustrate different I and ID responses (**Figure 6A-B**). We quantified the MI for all responsive glomerulus-odor pairings except for exclusively suppressed glomeruli (D) because they are assigned a strongly negative MI value (**Figure 6C**). Glomeruli binned into different MI ranges illustrate the heterogeneity of ID responses across the MTC population (**Figure 6C**). Within the population of non-suppressed MTC glomeruli, 53% exhibited some degree of non-monotonicity (**Figure 6D**). Importantly, the MI metric was significantly correlated with the slope of the concentration-response relationship, suggesting it accurately captures the general behavior of the different glomeruli in ($r = 0.6$, $p < 0.0001$), and because it incorporates response

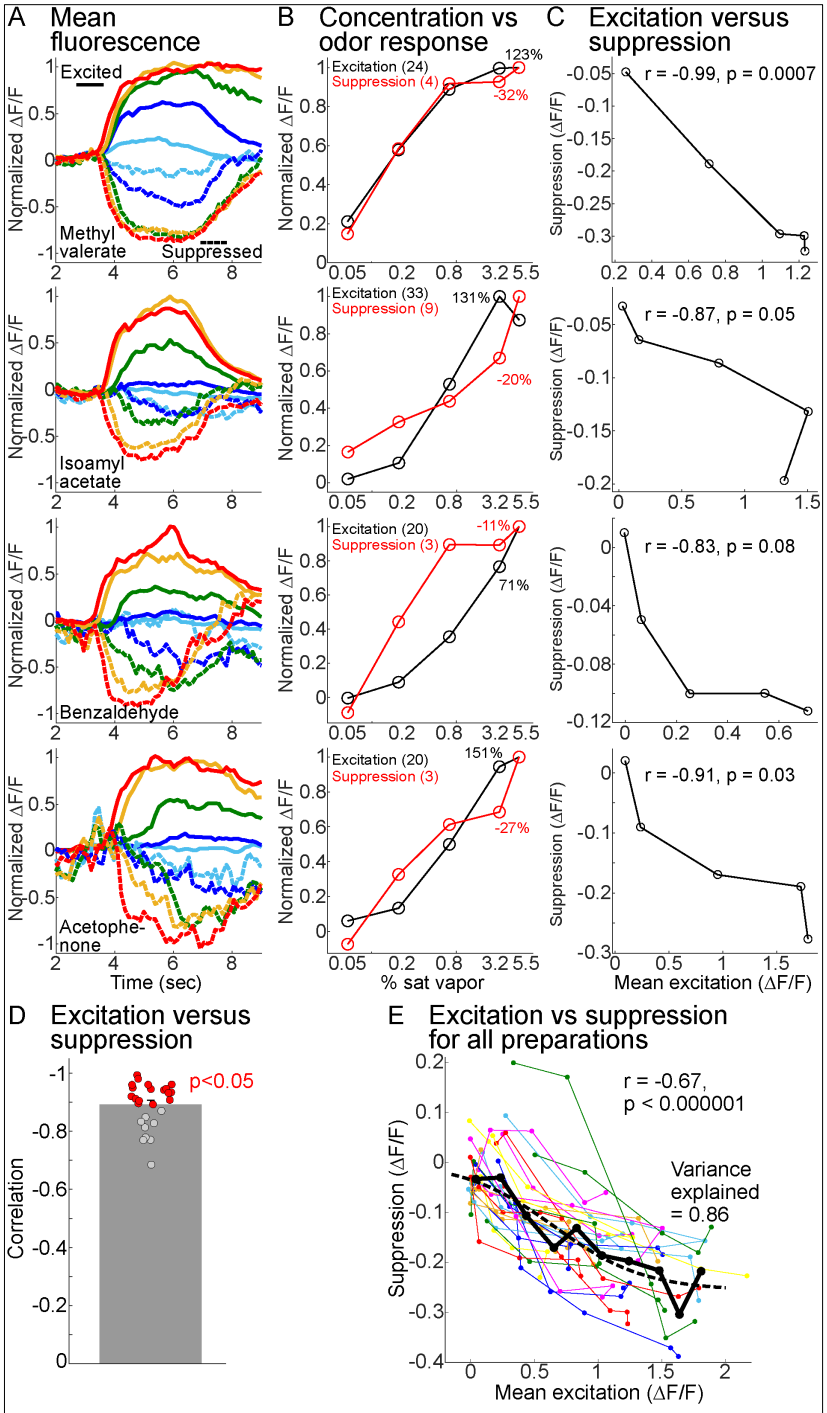

Figure 5: (**A-C**) Mean fluorescence time course of excited (solid traces) and suppressed (dashed traces) glomeruli (**A**), concentration versus normalized ΔF/F (**B**), and excitation versus suppression (**C**) for four preparations. The number of glomeruli averaged together and the maximum ΔF/F values are indicated in subpanel **B**. (**D**) Correlation between excitation and suppression for each preparation. (**E**) Mean excitation vs suppression for all preparations. Each individual point is the average of all the excited and suppressed glomeruli within a field of view for one concentration-odor pairing. Measurements from the same preparation-odor pairing are connected with a line. The individual points were binned (solid black line and black circles) and fit to a sigmoid (dashed line).

variability at each concentration to assign a value, provides an unbiased approach to defining the two categories (see Eq. 6).

We quantified the sensitivity of each MTC glomerulus with piecewise linear interpolation of each concentration-response relationship which was used to quantify the concentration evoking the half maximum response (**Figure 6A-B**, dashed vertical lines). In this analysis, glomeruli in which the response to the lowest concentration was greater than the half-maximum were assigned a value of 0.05% (e.g., **Figure 6B**, e.g., roi 9). ID glomeruli with more negative MI values tended to have lower half-maximum values in our exemplar preparations (**Figure 6A-B**, vertical lines), and across the population (**Figure 6E**, left panel, 324 glomerulus-odor pairings across 17 preparation-odor pairings). This relationship was significantly correlated (r = 0.48, p < 0.0001), and the half-maximum value of I glomeruli was significantly higher than ID glomeruli (**Figure 6E**, right panel, *p <= 0.00046 for all comparisons with MI = 0*). Thus, MTC glomeruli with ID responses tend to reach their half maximum response at lower concentrations than those exhibiting monotonically increasing relationships with odor concentration.

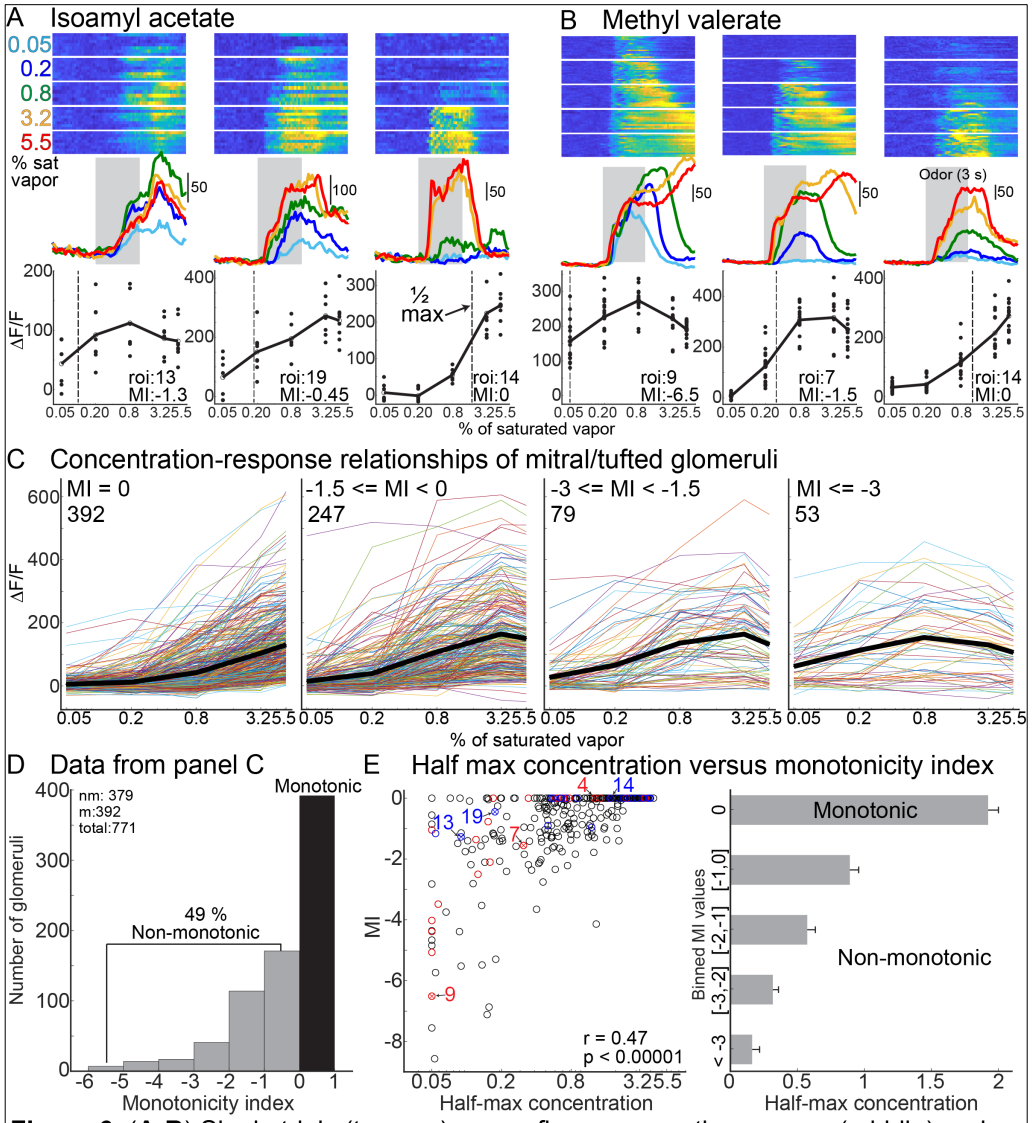

Figure 6: (**A-B**) Single trials (top row), mean fluorescence time course (middle) and mean concentration-response relationships (bottom) for three MTC glomeruli in two preparation-odor pairings. The vertical lines in the bottom subpanel of **A-B** indicate the half-maximum concentration. (**C**) Concentration response relationships for all responsive MTC glomeruli from all preparations binned by their MI, with the mean indicated with a black line. The number of glomeruli in each bin is in the top left of each panel. (**D**) Histogram of MI values from panel **C**. (**E**) The relationship between half-maximum concentration and MI. The colored circles in the left subpanel indicate measurements from the glomeruli in panels **A-B**.

***Non-monotonic MTC glomerular outputs originate from higher affinity ORN inputs*.**

The result that MTC glomeruli with smaller half-maximum values tend to be more non-monotonic is consistent with the model predictions (**Figure 6E**). However, a stronger and more direct test would involve systematically relating odor affinity to glomerular response profiles by functionally

imaging ORN and MTC glomeruli. Therefore, we generated a transgenic mouse in which GCaMP6s was expressed in the ORNs, and jRCaMP1b was selectively expressed in MTCs and their apical dendrites innervating the glomerular layer (**Figure 7A-B**). *In vivo* experiments were performed in

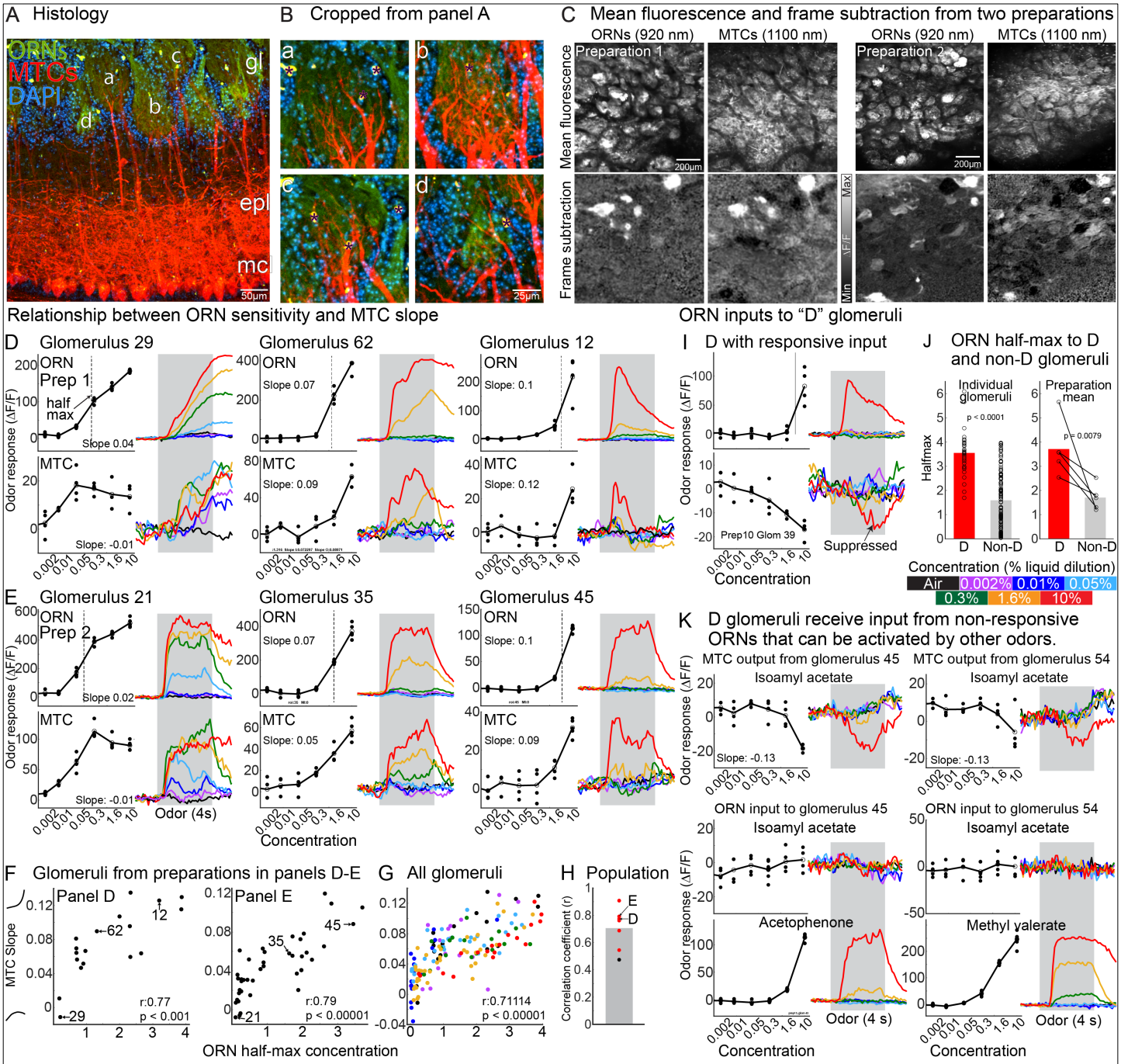

Figure 7: Measuring the olfactory bulb input-output transformation using 2-photon imaging. (**A**-**B**) Histology from a transgenic mouse expressing GCaMP6s in the ORNs, and jRCaMP1b in the MTCs. The bright yellow spots indicated with asterisks are lipofuscin autofluorescence. (**C**) Mean fluorescence and frame subtraction odor responses from the ORNs (imaged using 920 nm excitation) and MTCs (imaged using 1100 nm excitation) in 2 mouse preparations. (**D-E**) Input-output measurements from three glomeruli from two different mouse preparations. The glomeruli are sorted from lowest (most sensitive) to highest (least sensitive) half-maximum concentration value. (**F-H**) The correlation between ORN half- maximum and the slope of the MTC concentration-response relationship for glomeruli in the preparations in panels **D-E (F)**, and for all glomeruli in 8 preparation-odor pairings (**G**). (**H**) Mean correlation for each preparation-odor pairing. (**I**) An MTC glomerulus with a D concentration-response relationship that receives input from an ORN with a high half-maximum concentration. (**J**) Mean half-maximum value of all individual ORN glomeruli with D responses, and for all non-D glomeruli in the same preparation-odor pairings (left) and the mean for each preparation (right). (**K**) Examples of two MTC glomeruli with D responses that received ORN input that was not responsive to the same odor (isoamyl acetate), but could be activated by other odors (bottom, acetophenone and methyl valerate).

awake mice in which the dorsal OB was selectively illuminated with 920 nm to measure GCaMP fluorescence, and 1100 nm to measure jRCaMP1b fluorescence (**Figure 7C**, *top row illustrates the mean fluorescence from two different preparations*). In an abundance of caution, we performed all measurements of ORNs and MTCs in separate imaging trials that were illuminated with 920 nm or 1100 nm, respectively, due to the relatively long emission tail present for GCaMP (Akerboom et al., 2012). Imaging trials carried out at 920 nm and 1100 nm are hereafter referred to as ORN and MTC measurements, respectively. Odor responses were measured in 4 different mouse preparations to methyl valerate, isoamyl acetate, acetophenone and methyl salicylate delivered at 6 liquid dilutions ranging from 0.002% to 10% and air (a total of 8 preparation-odor pairings). A frame subtraction analysis revealed that odors evoked changes in glomerular sized regions of interest in both the ORN and MTC measurements (**Figure 7C**, *bottom row*).

The ORN and MTC odor response time course and corresponding concentration-response relationships are illustrated for 3 glomeruli from 2 different preparation-odor pairings (**Figure 7D-E**). The most sensitive ORN glomeruli often had correspondingly non-monotonic MTC outputs with small and sometimes negative slopes (**Figure 7D-E**, left most panels). We quantified the affinity of each ORN glomerulus by measuring the half-maximum value of the concentration-response relationship (e.g., **Figure 7D**, *vertical lines in the top row*), and the steepness of each MTC glomerulus by measuring the linear slope of the concentration-response relationship. The relationship between ORN affinity and MTC slope is illustrated for the two preparations in panels **D-E** in **Figure 7F** and was significantly correlated when combining all tested glomeruli from 8 preparation-odor pairings (**Figure 7G**, N = 159 glomeruli, glomeruli from different preparation-odor pairings are indicated by color). Finally, this relationship was significantly correlated in 7/8 preparation-odor pairings in the data set (**Figure 7H**).

***Decreasing MTC glomeruli originate from lower affinity ORN inputs*.**

Another prediction is that D MTC glomeruli are the consequence of input from low affinity ORNs with more sigmoidal concentration-response relationships, in which the rising levels of lateral inhibition exceed the feed-forward ORN excitation. We tested this prediction by measuring the input-output relationship of MTC glomeruli that were clearly suppressed by the odor at the highest concentration (e.g., **Figure 7I**, *output*). Our data set included 64 MTC glomeruli from 5 preparation-odor pairings (3 different animals) that were suppressed by the odor in response to the highest tested concentration with a mean Z-Score change of 5.9 ± 0.4 from baseline (**Figure 7I**, output). Of the MTC glomeruli with suppressed odor responses, 39/64 had an ORN odor responsive to at least one concentration with a minimum change of 5 standard deviations above baseline (e.g., **Figure 7I**, *input*). The odor-responsive inputs to the D MTC glomeruli had a mean half-maximum concentration of 3.4 ± 0.2, which was significantly larger than the half-maximum concentration of all other glomeruli when collapsing across all 5 preparation-odor pairings, or when comparing each preparation-odor pairing individually (**Figure 7J**). Interestingly, the remaining 25/64 D MTC glomeruli originated from ORN inputs that were non-responsive to the same odor (**Figure 7K**, *compare response of MTC and ORN to isoamyl acetate*). In the subset of the non-responsive inputs that were tested to multiple odors, most could be activated by another odor (10/13) (**Figure 7K**, *compare response of ORN to*

isoamyl acetate and acetophenone or methyl valerate). This indicates the lack of an ORN response to isoamyl acetate was not due to poor labeling or other methodological explanations. Together these results are consistent with the idea that D glomeruli of MTC are primarily innervated by lower affinity ORN glomeruli, which is consistent with the model predictions.

Discussion.

We generated a model of the OB input-output transformation that yielded predictions about how the MTC output of individual glomeruli is shaped by intraglomerular and interglomerular mechanisms. Different ORNs were transformed into different output response types that were determined by the Hill coefficient and half-activation value. Notably, our model predicted the presence of ID responses, which depended on lateral inhibition, were heterogeneous, and originated from higher affinity ORN input (**Figure 1**). *In vivo* measurements from MTC glomeruli revealed that higher concentrations activated increasing numbers of glomeruli, which exhibited a range of different concentration-response categories that were generally consistent with the model predictions, and which were present when measurements were performed using 3 different optical sensors (**Figure 3** and **Supplementary Figure S2**). Different odors evoked different response categories in 60% of glomerulus-odor pairings, suggesting that the concentration-response function of each MTC glomerulus is driven by network activity (**Figure 4**). Higher concentrations increased the mean level of excitation, which was significantly correlated with the magnitude of suppression present in other glomeruli in the same field of view (**Figure 5**). The model predictions suggest that ID responses are common, heterogeneous, and the consequence of rising levels of lateral inhibition that will begin to suppress sensitive and saturating ORN inputs. We performed dual-color 2-photon Ca^{2+} imaging from ORNs and MTCs in the same glomeruli to confirm this prediction (**Figure 7D-H**). Finally, we observed D responses in which glomeruli were exclusively innervated by low affinity or non-responsive ORN inputs, a result that is consistent with rising levels of lateral inhibition (**Figure 7I-K**). The modeling and experimental results indicate that MTC glomerular output is a complex mix of the overall balance of excitation and inhibition innervating that glomerulus.

Rationale for our modeling choices.

A fundamental assumption of the model is that the response function of periglomerular cells (PG) that provide local inhibition is left-shifted relative to that of mitral cells and has a lower saturating level (**Figure 1B**). This provides local half-hat coding, so that weaker input signals are suppressed while stronger ones get through. This is a key element of the model for olfactory coding hypothesized by Cleland[17,18]. Although this model has some experimental support, it would be strengthened by future experiments that directly compare the concentration sensitivity of local interneurons with mitral/tufted cells innervating the same glomerulus (e.g., as done for ORNs and MTCs in **Figure 7**)[21,22,38,53,54].

Another fundamental assumption is that there is lateral inhibition that increases with the odor concentration (the dashed curve in **Figure 1C** and **Supplemental Figure S1C**). Without this lateral inhibition the model produces only two response types: I and DI (**Supplemental Figure S1B**). If the half-hat assumption is incorrect, and PG cells are actually activated at higher odor concentrations than the mitral cells, then ID mitral cell responses could be produced with local inhibition alone, but in

that case DI responses would not be produced through local inhibition. The most parsimonious hypothesis is then that the PG activation function is left-shifted, and primarily responsible for the suppression in DI responses, while lateral inhibition is responsible for the suppression at higher odor concentrations and thereby yielding ID responses.

Our model implements interglomerular lateral inhibition by means of divisive normalization, a well-established mechanism for implementing gain control and contrast enhancement in sensory systems[23]. The most widely recognized example is in the visual system, as described by Heeger (1992), where neural responses are modeled as the ratio of input to the summed activity of a pool of neurons (plus a constant). This principle underlies our formulation of normalized ORN activity in Equation (2). Moreover, divisive mechanisms have been observed or proposed in multiple sensory modalities, including olfactory, auditory, and somatosensory systems[23,25,55]. In the olfactory system, interglomerular lateral inhibition is thought to implement a normalization mechanism that can make the glomerular activation pattern more stable across different concentrations[17,18,24,56]. Support for the existence of this mechanism has been shown anatomically and functionally as well[11,18,25,28,36,57-59]. The extent and structure of interglomerular inhibitory coupling is unclear[28,37,38]. Although we find in model simulations that the general categories of response types remain even when the normalization was performed using a selective subset of ORNs (**Supplemental Figure S1C-D**), future studies are needed that systematically compare how different normalization methods match empirical data. Given this broad precedent, we believe that modeling interglomerular inhibition as a divisive process is a reasonable and biologically plausible assumption.

Although we have schematized it as such, the specifics of our model do not require that lateral inhibition function presynaptically at the level of ORNs. The general effect of lateral inhibition in our model only needs to be presynaptic to the mitral cells to function in a similar way. Indeed, recent studies have shown that lateral inhibition can occur presynaptically to mitral cells through an indirect external tufted cell pathway[28]. Therefore, it is possible that the “interglomerular” inhibition in our model could reflect a combination of lateral presynaptic inhibition, lateral inhibition occurring at other levels of the bulb including through multi-synaptic pathways presynaptic to the MTCs, through granule cell mediated lateral inhibition, and even feedback from other brain areas[28,60-66].

Comparison with previous studies.

The presence of both linear and non-linear response types is in contrast with two prior studies reporting that MTC glomeruli exhibit exclusively monotonic concentration-response relationships[11,39]. Because monotonic and non-monotonic response types were often present in the same imaging field of view, the non-monotonic responses cannot be explained as technical limitations associated with our olfactometer, variations in the animal’s respiration, or odor chemistry. In addition, as the model shows, non-monotonic glomerular responses would be expected given what is known about local and interglomerular inhibition (**Figure 1**)[56]. We propose that these differences primarily reflect the use of epifluorescence versus 2-photon microscopy, which rejects significantly more out-of-focus fluorescence. Epifluorescence measurements from a region of interest will likely reflect a complicated average of the neighboring pixels, which **Figure 4** illustrates can include a combination of I, D, DI and ID glomeruli[67]. This is also supported by the observation that MTC glomeruli exhibit less steep

concentration-response relationships than their corresponding olfactory receptor neuron input when using epifluorescence imaging[11,12,68].

The heterogeneity of non-monotonic response types is also different from that described in recent experimental and modeling studies[37,38], in which a much smaller proportion of measurements exhibited non-monotonic responses. However, the experimental data in those studies were collected over a much smaller concentration range in anesthetized animals, which may have reduced the ability to detect changes that would occur over a larger range. While the study of Zavitz et al., 2020 captured the monotonic responses reported in [38], they did not account for the non-monotonic responses that were so frequent in our data.

Current models of how inhibitory circuits are shaped by excitation propose that inhibition either increases broadly across the glomerular population in a manner that scales with the magnitude of excitatory input, or increases selectively[24,28,37,38]. ID responses have been rarely described at the level of the input to the olfactory bulb[9-11,27,49,52,69-71]. Our theoretical and experimental results suggest that ID glomeruli likely reflect processing that occurs within the OB as higher affinity ORN input saturates and is weakened due to rising lateral inhibition (**Figures 1**, **6** and **7**). The result that higher levels of suppression are significantly correlated with increasing excitation is consistent with studies indicating that the responses of interneurons that mediate lateral connectivity exhibit activity that scales with increasing odor concentrations[12,28,58].

However, another study reported that the amount of excitation in MTC glomeruli was only weakly predictive of the amount of suppression[38]. We propose that a few methodological differences can explain the different conclusions. Our study sampled each glomerular field of view across a large range of odor concentrations, which increased the likelihood that we would observe glomeruli exhibiting this relationship. Additionally, glomeruli that were suppressed at the highest concentration were selected for analysis and their responses to each concentration were analyzed even if they were non-responsive at lower concentrations. This facilitated the identification of glomeruli with graded transitions from non-responsive to suppressed. Finally, we excluded glomeruli that we categorized as DI, which typically responded with suppression to lower concentrations, and transitioned to excitation at higher concentrations.

Our finding that more than half of the MTC glomeruli exhibit monotonic concentration-response relationships suggests it is ubiquitous. We also found that most MTC glomeruli exhibiting monotonic concentration-response relationships were well fit by the Hill equation and have Hill coefficients consistent with previous ORN measurements[9-11,49]. This does not mean that these MTC glomeruli are not affected by inhibitory input. In fact, in the model all glomeruli are subject to both local and lateral inhibition, but in many cases the concentration-response function is monotonically increasing (**Figure 1D**, I). Future studies with a more comprehensive analysis of the olfactory bulb input-output transformation alters concentration-response relationships are required to resolve the question of how each individual glomerulus is distinctly impacted by OB processing.

Methodological considerations.

Sensor considerations. Because action potentials trigger a rapid influx of calcium into neurons, calcium indicators provide an indirect report of neural activity. Calcium sensors each have distinct

biophysical properties, which include their affinity for calcium, and the slope of this binding relationship. GCaMP6f, with a calcium affinity of 375 nM and a Hill coefficient of 2.27 ± 0.1, has a well characterized monotonic sigmoidal relationship between calcium binding and ΔF/F[72-74]. Additionally, changes in spiking activity in mitral cells evoke relatively linear changes in GCaMP ΔF/F[73,75]. Therefore, non-monotonic ID and DI responses cannot be explained by the biophysics of the GCaMP6f sensor. This conclusion is strongly supported by our result that ID and DI responses were present in additional data sets measured using two different calcium indicators with different calcium affinities and Hill coefficients, jRCaMP1b (Kd: 712 ± 9 nM; n = 1.6)[76] and jGCaMP8m (Kd: 108 ± 3 nM, n = 1.92 ± 0.12)[77] (**Supplementary Figure S3**).

Functional relevance of non-monotonic concentration-response relationships.

Non-monotonic intensity relationships ("ID" in our study) have been described in other sensory systems as a mechanism by which the brain can encode absolute or relative intensity differences[78-81]. In the auditory cortex, non-monotonic neurons exhibit unique characteristics including being particularly sensitive to behavioral training and exhibiting unique adaptive properties[82-84]. Although our model indicates that these glomeruli are a natural consequence of the interplay between intra- and interglomerular inhibition, it remains to be tested whether these strongly suppressed glomeruli are functionally unique.

One advantage of having four distinct response types to an odor over a range of concentrations is that it provides a broader range of coverage of the MTC state space. As a simple example we consider only three glomeruli, with output MTC_1, MTC_2, and MTC_3. The response amplitude of each to an odor at a given concentration would be a point in the MTC_1-MTC_2-MTC_3 state space, and the response to that odor over a range of concentrations would be a set of points that can be thought of as a directed curve in that space, which we refer to as a trajectory (**Supplementary Figure S4**). The neural coding of an odor across concentrations in the olfactory bulb would then be a trajectory in the MTC state space. The response to a second odor over a similar range of concentrations would produce a different trajectory. In both cases, the trajectory should be considered a cloud of points that reflect variations in the fluctuations of molecular components present in natural odor stimuli (whether due to differences in chemistry or environmental interactions). An animal would learn to recognize an odor in a concentration invariant manner as the population activation along that trajectory based on experience.

To illustrate how different response types impact coverage of the MTC state space we show a collection of trajectories all having an I response to an odor (black curves in **Supplementary Figure S4**) and an equal number having a mix of monotonic and non-monotonic response types (red curves in **Supplementary Figure S4**). Each trajectory is based on calcium measurements from 3 glomeruli. When the responses are all of the I type they cover only a small region of the state space. In contrast, when non-monotonic responses are included, the coverage is much more extensive. The greater coverage makes it easier to discriminate one odor from another, and even though the dimension of the actual MTC state space is much larger than 3 (equal to the number of different receptor types), it is still advantageous to increase the coverage of that space, as is done by having different response types to odors.

Future studies and conclusions.

It is necessary to know the concentration-response relationships of the input to each glomerulus to further understand the transformation occurring within each glomerulus. Knowing the input-output relationship will allow for additional tests of our proposed model, including a more precise test of the relationship between affinity and ID responses (**Figure 1**). Importantly, the model predicted that DI responses could be due to intraglomerular inhibition from PG interneurons, while ID responses required lateral inhibition. Future studies are needed to test this hypothesis by measuring concentration-response relationships before and after selectively manipulating the different cell types involved in these two different computations[28]. To understand the relationship between excitation, suppression and how they are related spatially, experiments are required that incorporate more precise control over the input activation pattern to the brain[85-87].

In the analysis of our fluorescence data, we focus on the amplitude of the calcium response rather than the timing, and our mathematical model likewise is independent of response timing. It is likely, however, that timing is also important for the neural coding of odor[88-91]. Indeed, the "primacy coding" scheme hypothesizes that only those receptors that act earliest are responsible for the neural coding of an odor[92]. In this model, whether the MTC response is monotonic or non-monotonic is of little relevance, since what matters is the timing of the response. This coding strategy greatly limits the potential that is available through the variety of amplitude responses (I, D, DI, ID) produced at different odor concentrations that we and others have found. In our view, both timing and amplitude provide useful information that can be employed in the neural coding of odor over different concentrations, and are likely to both be employed in some way. Temporal dynamics of glomerular responses to an odor could be incorporated into the model by using time-dependent differential equations, both at the level of ORNs and MTCs.

The present study used monomolecular odors, yet natural odors are often mixtures of different components that can interact antagonistically at the ORN receptor level[7,9,69]. An odor mixture that causes antagonism in a particular OR type will necessarily right shift its ORN binding curve (i.e., make it lower affinity). At the same time, the mixture will increase the magnitude of lateral inhibition by activating other OR types (**Figure 1C**). One prediction from our model is therefore that antagonized ORNs will result in MTCs outputs that shift towards the D and DI categories (moving downward in **Figure 1E**). Thus, we suggest that antagonism or mixtures need not be thought of as interfering with the signal that an odorant sends to a particular MTC, but maybe more importantly, changes the way that the MTC codes for that odor. For example, without antagonism at the receptor level the glomerulus may have had an I response (black region in **Figure 1E**). With antagonism, it could shift to a DI response (green region below the black region in **Figure 1E**).

The model can also be further developed to consider the impact of different interglomerular inhibitory network structures[37]. We performed preliminary work in this direction, replacing all-to-all coupling with random sampling of the glomeruli providing the lateral inhibition. All four response types were reproduced with this network structure (**Supplemental Figure S1**). However, much more can be done to test the effects of different inhibitory network structures. Spatial effects may be heterogeneous, for example, and there could be spatial or functional clustering, so that the lateral

inhibition targeted to a glomerulus could be preferentially from nearby glomeruli, or from glomeruli responsive to very distinct odors. The primary conclusion from this study is that non-monotonic concentration-responses to MTC glomeruli are quite common, and the model shows that these are in fact expected given the ways that local and lateral inhibition can shape MTC activity. We believe that the non-monotonic response types are useful in the discrimination of different odors.

Figure Legends

Figure 1: (**A**) Model of the glomerular input-output transformation. (**B**) Local inhibition alone generates a half-hat response in MTCs. (**C**) The population of ORNs in the model (thin lines) used to calculate the normalization function (dashed line). (**D**) The concentration-response relationships of four ORNs (left) and their corresponding MTC output (right) reflecting both local and lateral inhibition. Output responses were categorized based on the shape of the concentration-response relationship: I, increasing; ID, increasing then decreasing; DI, decreasing then increasing; D, decreasing. (**E**) MTC responses for different ORN Hill coefficients and half-activation values. (**F**) The decrease from the maximum to the terminal odorant concentration value for combinations of Hill coefficients and half-activation values that result in an ID response.

Figure 2: (**A**) Mean fluorescence (left subpanel) and frame subtractions illustrating MTC activation at different concentrations in 3 preparations (rows). The intensity scale is fixed within each preparation. The arrows highlight glomeruli with increasing (I), decreasing (D), increasing-decreasing (ID) and decreasing-increasing (DI) concentration-response relationships. (**B**) Fluorescence time course from all glomerulus-odor pairings. The color scale is fixed across the 5 concentrations. (**C**) Response to all glomeruli for each odor sorted by the maximum response to each concentration (colors). (**D**) Same arrangement as panel **C** except that glomeruli are sorted by the maximum response to the highest concentration. (**E**) Data from panel **D** cropped to visualize suppressed glomeruli. (**F**-**H**) Descriptive statistics.

Figure 3: (**A**-**D**) Single trials (top), mean fluorescence time course (middle) and concentration-response relationships with points indicating the response amplitudes from the single trials for four different preparations. (**E**) Mean concentration-response relationships for each preparation-odor pairing for each response type (1st four subpanels), and across all glomeruli in each field of view (right-most subpanel). (**F**) Mean fluorescence time course from all glomeruli in each category.

Figure 4: (**A**) Maps of glomerular odor responses ($\Delta F/F$) in different preparations in response to different odors. The color scale is fixed across all concentrations for each preparation-odor pairing. Glomeruli that do not respond to any concentration are indicated with a hatched overlay. (**B**) Maps of glomerular response categories: I, Increasing, D, Decreasing; DI, Decreasing then increasing; ID, Increasing then decreasing, nr, Non-responsive; O, Other type not clearly associated with any category. IA, isoamyl acetate; BZA, benzaldehyde; ACP, acetophenone; MV, methyl valerate. (**C**) A

histogram and network graph illustrate how changing the odor changed the proportions of each response type. (**D**) Network graph illustrating transitions between categories as a function of odor change.

Figure 5: (**A**-**C**) Mean fluorescence time course of excited (solid traces) and suppressed (dashed traces) glomeruli (**A**), concentration versus normalized ∆F/F (**B**), and excitation versus suppression (**C**) for four preparations. The number of glomeruli averaged together and the maximum ∆F/F values are indicated in subpanel **B**. (**D**) Correlation between excitation and suppression for each preparation. (**E**) Mean excitation vs suppression for all preparations. Each individual point is the average of all the excited and suppressed glomeruli within a field of view for one concentration-odor pairing. Measurements from the same preparation-odor pairing are connected with a line. The individual points were binned (solid black line and black circles) and fit to a sigmoid (dashed line).

Figure 6: (**A**-**B**) Single trials (top row), mean fluorescence time course (middle) and mean concentration-response relationships (bottom) for three MTC glomeruli in two preparation-odor pairings. The vertical lines in the bottom subpanel of **A**-**B** indicate the half-maximum concentration. (**C**) Concentration response relationships for all responsive MTC glomeruli from all preparations binned by their MI, with the mean indicated with a black line. The number of glomeruli in each bin is in the top left of each panel. (**D**) Histogram of MI values from panel **C**. (**E**) The relationship between half-maximum concentration and MI. The colored circles in the left subpanel indicate measurements from the preparations in panels **A**-**B**.

Figure 7: (**A**-**B**) Histology from a transgenic mouse expressing GCaMP6s in the ORNs, and jRCaMP1b in the MTCs. The bright yellow spots indicated with asterisks are lipofuscin autofluorescence. (**C**) Mean fluorescence and frame subtraction odor responses from the ORNs (imaged using 920 nm excitation) and MTCs (imaged using 1100 nm excitation) in 2 mouse preparations. (**D**-**E**) Input-output measurements from three glomeruli from two different mouse preparations. The glomeruli are sorted from lowest (most sensitive) to highest (least sensitive) half-maximum concentration value. (**F**-**H**) The correlation between ORN half-maximum and the slope of the MTC concentration-response relationship for glomeruli in the preparations in panels **D**-**E** (**F**), and for all glomeruli in 8 preparation-odor pairings (**G**). (**H**) Correlation coefficient of each preparation for all 8 preparations. (**I**) An MTC glomerulus with a D concentration-response relationship that receives input from ORN with a high half-maximum concentration. (**J**) Mean half-maximum value of all individual ORN glomeruli with D responses, and for all non-D glomeruli in the same preparation-odor pairings (left) and the mean for each preparation (right). (**K**) Examples of two MTC glomeruli with D responses that received ORN input that was not responsive to the same odor (isoamyl acetate), but could be activated by other odors (bottom, acetophenone and methyl valerate).

Supplementary Figure S1: Input and output curves from the mathematical model. (**A**) Four exemplar ORN concentration-response functions. To facilitate direct comparison, these signals are identical to those displayed in **Figure 1D**. (**B**) The four inputs from panel **A** have been processed by the local

inhibition circuit (only), resulting in three I and one DI MTC response functions. Importantly, no ID responses were generated in the absence of lateral inhibition. (**C**) Three different ORN normalization functions used to implemental lateral inhibition. The solid "μ_{global}" distribution is identical to the black dashed line in **Figure 1C**. Randomly sampling and then averaging 5 and 10 signals from that figure's ORN population yielded the "$\mu_{Random5}$" and "$\mu_{Random10}$" distributions, respectively (*different dashed lines*). (**D**) The four inputs from panel **A** processed using local inhibition and lateral inhibition implemented via the different normalization functions in panel **C**. All four MTC categories were present irrespective of which normalizing function was selected.

Supplementary Figure S2: (**A**) A transgenic cross between Tbx21-Cre and the TIGRE2-jGCaMP8m transgenic lines illustrating jGCaMP8m expression in mitral/tufted cells. gl, glomerular layer; mcl, mitral cell layer.

Supplementary Figure S3: MTC glomerular responses with increasing, decreasing, decreasing-increasing and increasing-decreasing response categories measured with jGCaMP8m (**A**) and jRCaMP1b (**B**).

Supplementary Figure S4: Proposed model of how the non-canonical response types influence odor coding in the MTC state space. Each line in this model illustrates the response of 3 MTC glomeruli to a single odor across concentration changes. Concentration changes are represented as the changing transparency of each line. MTC glomeruli with only increasing responses tended to cluster together in perceptual space (black lines). In contrast, MTC glomeruli with different response categories had response trajectories that diverged from one another. Each panel illustrates the projections from a different angle.

Bibliography

1. Carandini, M. (2012). From circuits to behavior: a bridge too far? Nat Neurosci *15*, 507-509. 10.1038/nn.3043.
2. Kanter, B.R., Lykken, C.M., Moser, E.I., and Moser, M.B. (2022). Neuroscience in the 21st century: circuits, computation, and behaviour. Lancet Neurol *21*, 19-21. 10.1016/S1474-4422(21)00427-0.
3. Langdon, C., Genkin, M., and Engel, T.A. (2023). A unifying perspective on neural manifolds and circuits for cognition. Nat Rev Neurosci *24*, 363-377. 10.1038/s41583-023-00693-x.
4. Buck, L., and Axel, R. (1991). A novel multigene family may encode odorant receptors: a molecular basis for odor recognition. Cell *65*, 175-187. 0092-8674(91)90418-X [pii].
5. Malnic, B., Hirono, J., Sato, T., and Buck, L.B. (1999). Combinatorial receptor codes for odors. Cell *96*, 713-723. S0092-8674(00)80581-4 [pii].
6. Araneda, R.C., Kini, A.D., and Firestein, S. (2000). The molecular receptive range of an odorant receptor. Nat Neurosci *3*, 1248-1255. 10.1038/81774.
7. Xu, L., Li, W., Voleti, V., Zou, D.J., Hillman, E.M.C., and Firestein, S. (2020). Widespread receptor-driven modulation in peripheral olfactory coding. Science *368*. 10.1126/science.aaz5390.
8. Reisert, J., and Matthews, H.R. (1999). Adaptation of the odour-induced response in frog olfactory receptor cells. J Physiol *519 Pt 3*, 801-813. 10.1111/j.1469-7793.1999.0801n.x.
9. Zak, J.D., Reddy, G., Vergassola, M., and Murthy, V.N. (2020). Antagonistic odor interactions in olfactory sensory neurons are widespread in freely breathing mice. Nat Commun *11*, 3350. 10.1038/s41467-020-17124-5.
10. Wachowiak, M., and Cohen, L.B. (2001). Representation of odorants by receptor neuron input to the mouse olfactory bulb. Neuron *32*, 723-735. S0896-6273(01)00506-2 [pii].
11. Storace, D.A., and Cohen, L.B. (2017). Measuring the olfactory bulb input-output transformation reveals a contribution to the perception of odorant concentration invariance. Nat Commun *8*, 81. 10.1038/s41467-017-00036-2.
12. Storace, D.A., Cohen, L.B., and Choi, Y. (2019). Using Genetically Encoded Voltage Indicators (GEVIs) to Study the Input-Output Transformation of the Mammalian Olfactory Bulb. Front Cell Neurosci *13*, 342. 10.3389/fncel.2019.00342.
13. Hu, X.S., Ikegami, K., Vihani, A., Zhu, K.W., Zapata, M., de March, C., Do, M., Vaidya, N., Kucera, G., Bock, C., et al. (2020). Concentration-dependent recruitment of mammalian odorant receptors. eNeuro. 10.1523/eneuro.0103-19.2019.
14. Nagayama, S., Enerva, A., Fletcher, M.L., Masurkar, A.V., Igarashi, K.M., Mori, K., and Chen, W.R. (2010). Differential axonal projection of mitral and tufted cells in the mouse main olfactory system. Front Neural Circuits *4*. 10.3389/fncir.2010.00120.
15. Igarashi, K.M., Ieki, N., An, M., Yamaguchi, Y., Nagayama, S., Kobayakawa, K., Kobayakawa, R., Tanifuji, M., Sakano, H., Chen, W.R., and Mori, K. (2012). Parallel mitral and tufted cell pathways route distinct odor information to different targets in the olfactory cortex. J Neurosci *32*, 7970-7985. 10.1523/jneurosci.0154-12.2012.
16. Chen, Y., Chen, X., Baserdem, B., Zhan, H., Li, Y., Davis, M.B., Kebschull, J.M., Zador, A.M., Koulakov, A.A., and Albeanu, D.F. (2022). High-throughput sequencing of single neuron projections reveals spatial organization in the olfactory cortex. Cell *185*, 4117-4134.e4128. 10.1016/j.cell.2022.09.038.
17. Cleland, T.A., and Sethupathy, P. (2006). Non-topographical contrast enhancement in the olfactory bulb. BMC Neurosci *7*, 7. 10.1186/1471-2202-7-7.
18. Cleland, T.A. (2010). Early transformations in odor representation. Trends Neurosci *33*, 130-139. 10.1016/j.tins.2009.12.004.
19. Parrish-Aungst, S., Shipley, M.T., Erdelyi, F., Szabo, G., and Puche, A.C. (2007). Quantitative analysis of neuronal diversity in the mouse olfactory bulb. J Comp Neurol *501*, 825-836. 10.1002/cne.21205.
20. Nagayama, S., Homma, R., and Imamura, F. (2014). Neuronal organization of olfactory bulb circuits. Front Neural Circuits *8*, 98. 10.3389/fncir.2014.00098.
21. Gire, D.H., and Schoppa, N.E. (2009). Control of on/off glomerular signaling by a local GABAergic microcircuit in the olfactory bulb. J Neurosci *29*, 13454-13464. 10.1523/jneurosci.2368-09.2009.

22. Shao, Z., Puche, A.C., Kiyokage, E., Szabo, G., and Shipley, M.T. (2009). Two GABAergic intraglomerular circuits differentially regulate tonic and phasic presynaptic inhibition of olfactory nerve terminals. J Neurophysiol *101*, 1988-2001. 10.1152/jn.91116.2008.
23. Carandini, M., and Heeger, D.J. (2011). Normalization as a canonical neural computation. Nat Rev Neurosci *13*, 51-62. 10.1038/nrn3136.
24. Cleland, T.A., Johnson, B.A., Leon, M., and Linster, C. (2007). Relational representation in the olfactory system. Proc Natl Acad Sci U S A *104*, 1953-1958. 10.1073/pnas.0608564104.
25. Olsen, S.R., Bhandawat, V., and Wilson, R.I. (2010). Divisive normalization in olfactory population codes. Neuron *66*, 287-299. 10.1016/j.neuron.2010.04.009.
26. McGann, J.P. (2013). Presynaptic inhibition of olfactory sensory neurons: new mechanisms and potential functions. Chem Senses *38*, 459-474. 10.1093/chemse/bjt018.
27. Martelli, C., and Storace, D.A. (2021). Stimulus Driven Functional Transformations in the Early Olfactory System. Frontiers in Cellular Neuroscience *15*. 10.3389/fncel.2021.684742.
28. Banerjee, A., Marbach, F., Anselmi, F., Koh, M.S., Davis, M.B., Garcia da Silva, P., Delevich, K., Oyibo, H.K., Gupta, P., Li, B., and Albeanu, D.F. (2015). An Interglomerular Circuit Gates Glomerular Output and Implements Gain Control in the Mouse Olfactory Bulb. Neuron *87*, 193-207. 10.1016/j.neuron.2015.06.019.
29. Firestein, S., Picco, C., and Menini, A. (1993). The relation between stimulus and response in olfactory receptor cells of the tiger salamander. J Physiol *468*, 1-10. 10.1113/jphysiol.1993.sp019756.
30. Kurahashi, T., and Menini, A. (1997). Mechanism of odorant adaptation in the olfactory receptor cell. Nature *385*, 725-729. 10.1038/385725a0.
31. Menini, A., Picco, C., and Firestein, S. (1995). Quantal-like current fluctuations induced by odorants in olfactory receptor cells. Nature *373*, 435-437. 10.1038/373435a0.
32. Mathews, D.F. (1972). Response patterns of single units in the olfactory bulb of the rat to odor. Brain Res *47*, 389-400. 10.1016/0006-8993(72)90647-6.
33. Meredith, M. (1986). Patterned response to odor in mammalian olfactory bulb: the influence of intensity. J Neurophysiol *56*, 572-597. 10.1152/jn.1986.56.3.572.
34. Mair, R.G. (1982). Response properties of rat olfactory bulb neurones. J Physiol *326*, 341-359. 10.1113/jphysiol.1982.sp014197.
35. Niessing, J., and Friedrich, R.W. (2010). Olfactory pattern classification by discrete neuronal network states. Nature *465*, 47-52. 10.1038/nature08961.
36. Shen, Y., Banerjee, A., Albeanu, D.F., and Navlakha, S. (2025). An evolutionarily conserved mechanism for reformatting odor concentration in early olfactory circuits. bioRxiv, 2025.2001.2023.634259. 10.1101/2025.01.23.634259.
37. Zavitz, D., Youngstrom, I.A., Borisyuk, A., and Wachowiak, M. (2020). Effect of Interglomerular Inhibitory Networks on Olfactory Bulb Odor Representations. J Neurosci *40*, 5954-5969. 10.1523/JNEUROSCI.0233-20.2020.
38. Economo, M.N., Hansen, K.R., and Wachowiak, M. (2016). Control of Mitral/Tufted Cell Output by Selective Inhibition among Olfactory Bulb Glomeruli. Neuron *91*, 397-411. 10.1016/j.neuron.2016.06.001.
39. Fletcher, M.L., Masurkar, A.V., Xing, J., Imamura, F., Xiong, W., Nagayama, S., Mutoh, H., Greer, C.A., Knopfel, T., and Chen, W.R. (2009). Optical imaging of postsynaptic odor representation in the glomerular layer of the mouse olfactory bulb. J Neurophysiol *102*, 817-830. 00020.2009 [pii] 10.1152/jn.00020.2009.
40. Subramanian, N., Leong, L.M., Salemi Mokri Boukani, P., and Storace, D.A. (2025). Recent odor experience selectively modulates olfactory sensitivity across the glomerular output in the mouse olfactory bulb. Chem Senses *50*. 10.1093/chemse/bjae045.
41. Daigle, T.L., Madisen, L., Hage, T.A., Valley, M.T., Knoblich, U., Larsen, R.S., Takeno, M.M., Huang, L., Gu, H., Larsen, R., et al. (2018). A Suite of Transgenic Driver and Reporter Mouse Lines with Enhanced Brain-Cell-Type Targeting and Functionality. Cell *174*, 465-480 e422. 10.1016/j.cell.2018.06.035.
42. Mitsui, S., Igarashi, K.M., Mori, K., and Yoshihara, Y. (2011). Genetic visualization of the secondary olfactory pathway in Tbx21 transgenic mice. Neural Syst Circuits *1*, 5. 10.1186/2042-1001-1-5.
43. Huang, J.S., Kunkhyen, T., Rangel, A.N., Brechbill, T.R., Gregory, J.D., Winson-Bushby, E.D., Liu, B., Avon, J.T., Muggleton, R.J., and Cheetham, C.E.J. (2022). Immature olfactory sensory neurons provide behaviourally relevant sensory input to the olfactory bulb. Nat Commun *13*, 6194. 10.1038/s41467-022-33967-6.

44. Yu, C.H., Yu, Y., Adsit, L.M., Chang, J.T., Barchini, J., Moberly, A.H., Benisty, H., Kim, J., Young, B.K., Heng, K., et al. (2024). The Cousa objective: a long-working distance air objective for multiphoton imaging in vivo. Nat Methods *21*, 132-141. 10.1038/s41592-023-02098-1.
45. Storace, D.A., and Cohen, L.B. (2021). The mammalian olfactory bulb contributes to the adaptation of odor responses: a second perceptual computation carried out by the bulb. eNeuro. 10.1523/ENEURO.0322-21.2021.
46. Escabí, M.A., Higgins, N.C., Galaburda, A.M., Rosen, G.D., and Read, H.L. (2007). Early cortical damage in rat somatosensory cortex alters acoustic feature representation in primary auditory cortex. Neuroscience *150*, 970-983. 10.1016/j.neuroscience.2007.07.054.
47. Higgins, N.C., Escabí, M.A., Rosen, G.D., Galaburda, A.M., and Read, H.L. (2008). Spectral processing deficits in belt auditory cortex following early postnatal lesions of somatosensory cortex. Neuroscience *153*, 535-549. 10.1016/j.neuroscience.2008.01.073.
48. Firestein, S., and Zufall, F. (1993). Membrane currents and mechanisms of olfactory transduction. Ciba Found Symp *179*, 115-126; discussion 126-130, 147-119. 10.1002/9780470514511.ch8.
49. Platisa, J., Zeng, H., Madisen, L., Cohen, L.B., Pieribone, V.A., and Storace, D.A. (2022). Voltage imaging in the olfactory bulb using transgenic mouse lines expressing the genetically encoded voltage indicator ArcLight. Sci Rep *12*, 1875. 10.1038/s41598-021-04482-3.
50. Fantana, A.L., Soucy, E.R., and Meister, M. (2008). Rat olfactory bulb mitral cells receive sparse glomerular inputs. Neuron *59*, 802-814. S0896-6273(08)00678-8 [pii] 10.1016/j.neuron.2008.07.039.
51. Verhagen, J.V., Wesson, D.W., Netoff, T.I., White, J.A., and Wachowiak, M. (2007). Sniffing controls an adaptive filter of sensory input to the olfactory bulb. Nat Neurosci *10*, 631-639. 10.1038/nn1892.
52. Lecoq, J., Tiret, P., and Charpak, S. (2009). Peripheral adaptation codes for high odor concentration in glomeruli. J Neurosci *29*, 3067-3072. 10.1523/jneurosci.6187-08.2009.
53. Pinching, A.J., and Powell, T.P. (1971). The neuropil of the glomeruli of the olfactory bulb. J Cell Sci *9*, 347-377. 10.1242/jcs.9.2.347.
54. White, E.L. (1972). Synaptic organization in the olfactory glomerulus of the mouse. Brain Res *37*, 69-80. 10.1016/0006-8993(72)90346-0.
55. Rabinowitz, N.C., Willmore, B.D., Schnupp, J.W., and King, A.J. (2011). Contrast gain control in auditory cortex. Neuron *70*, 1178-1191. 10.1016/j.neuron.2011.04.030.
56. Cleland, T.A., Chen, S.Y., Hozer, K.W., Ukatu, H.N., Wong, K.J., and Zheng, F. (2011). Sequential mechanisms underlying concentration invariance in biological olfaction. Front Neuroeng *4*, 21. 10.3389/fneng.2011.00021.
57. Aungst, J.L., Heyward, P.M., Puche, A.C., Karnup, S.V., Hayar, A., Szabo, G., and Shipley, M.T. (2003). Centre-surround inhibition among olfactory bulb glomeruli. Nature *426*, 623-629. 10.1038/nature02185 nature02185 [pii].
58. Zhu, P., Frank, T., and Friedrich, R.W. (2013). Equalization of odor representations by a network of electrically coupled inhibitory interneurons. Nat Neurosci *16*, 1678-1686. 10.1038/nn.3528.
59. Olsen, S.R., and Wilson, R.I. (2008). Lateral presynaptic inhibition mediates gain control in an olfactory circuit. Nature *452*, 956-960. 10.1038/nature06864.
60. Vucinic, D., Cohen, L.B., and Kosmidis, E.K. (2006). Interglomerular center-surround inhibition shapes odorant-evoked input to the mouse olfactory bulb in vivo. J Neurophysiol *95*, 1881-1887. 00918.2005 [pii] 10.1152/jn.00918.2005.
61. Otazu, G.H., Chae, H., Davis, M.B., and Albeanu, D.F. (2015). Cortical Feedback Decorrelates Olfactory Bulb Output in Awake Mice. Neuron *86*, 1461-1477. 10.1016/j.neuron.2015.05.023.
62. Zak, J.D., Reddy, G., Konanur, V., and Murthy, V.N. (2024). Distinct information conveyed to the olfactory bulb by feedforward input from the nose and feedback from the cortex. Nat Commun *15*, 3268. 10.1038/s41467-024-47366-6.
63. Petzold, G.C., Hagiwara, A., and Murthy, V.N. (2009). Serotonergic modulation of odor input to the mammalian olfactory bulb. Nat Neurosci *12*, 784-791. 10.1038/nn.2335.
64. Kapoor, V., Provost, A.C., Agarwal, P., and Murthy, V.N. (2016). Activation of raphe nuclei triggers rapid and distinct effects on parallel olfactory bulb output channels. Nat Neurosci *19*, 271-282. 10.1038/nn.4219.

65. Rothermel, M., Carey, R.M., Puche, A., Shipley, M.T., and Wachowiak, M. (2014). Cholinergic inputs from Basal forebrain add an excitatory bias to odor coding in the olfactory bulb. J Neurosci *34*, 4654-4664. 10.1523/jneurosci.5026-13.2014.
66. Rothermel, M., and Wachowiak, M. (2014). Functional imaging of cortical feedback projections to the olfactory bulb. Front Neural Circuits *8*, 73. 10.3389/fncir.2014.00073.
67. Orbach, H.S., and Cohen, L.B. (1983). Optical monitoring of activity from many areas of the in vitro and in vivo salamander olfactory bulb: a new method for studying functional organization in the vertebrate central nervous system. J Neurosci *3*, 2251-2262. 10.1523/JNEUROSCI.03-11-02251.1983.
68. Leong, L.M., and Storace, D.A. (2024). Imaging different cell populations in the mouse olfactory bulb using the genetically encoded voltage indicator ArcLight. Neurophotonics *11*, 033402. 10.1117/1.NPh.11.3.033402.
69. Inagaki, S., Iwata, R., Iwamoto, M., and Imai, T. (2020). Widespread Inhibition, Antagonism, and Synergy in Mouse Olfactory Sensory Neurons In Vivo. Cell Reports *31*. Unsp 107814 10.1016/J.Celrep.2020.107814.
70. Bozza, T., McGann, J.P., Mombaerts, P., and Wachowiak, M. (2004). In vivo imaging of neuronal activity by targeted expression of a genetically encoded probe in the mouse. Neuron *42*, 9-21.
71. Carey, R.M., Verhagen, J.V., Wesson, D.W., Pirez, N., and Wachowiak, M. (2009). Temporal structure of receptor neuron input to the olfactory bulb imaged in behaving rats. J Neurophysiol *101*, 1073-1088. 10.1152/jn.90902.2008.
72. Chen, T.W., Wardill, T.J., Sun, Y., Pulver, S.R., Renninger, S.L., Baohan, A., Schreiter, E.R., Kerr, R.A., Orger, M.B., Jayaraman, V., et al. (2013). Ultrasensitive fluorescent proteins for imaging neuronal activity. Nature *499*, 295-300. 10.1038/nature12354.
73. Badura, A., Sun, X.R., Giovannucci, A., Lynch, L.A., and Wang, S.S. (2014). Fast calcium sensor proteins for monitoring neural activity. Neurophotonics *1*, 025008. 10.1117/1.NPh.1.2.025008.
74. Helassa, N., Podor, B., Fine, A., and Torok, K. (2016). Design and mechanistic insight into ultrafast calcium indicators for monitoring intracellular calcium dynamics. Sci Rep *6*, 38276. 10.1038/srep38276.
75. Wachowiak, M., Economo, M.N., Diaz-Quesada, M., Brunert, D., Wesson, D.W., White, J.A., and Rothermel, M. (2013). Optical dissection of odor information processing in vivo using GCaMPs expressed in specified cell types of the olfactory bulb. J Neurosci *33*, 5285-5300. 10.1523/jneurosci.4824-12.2013.
76. Dana, H., Mohar, B., Sun, Y., Narayan, S., Gordus, A., Hasseman, J.P., Tsegaye, G., Holt, G.T., Hu, A., Walpita, D., et al. (2016). Sensitive red protein calcium indicators for imaging neural activity. Elife *5*. 10.7554/eLife.12727.
77. Zhang, Y., Rózsa, M., Liang, Y., Bushey, D., Wei, Z., Zheng, J., Reep, D., Broussard, G.J., Tsang, A., Tsegaye, G., et al. (2023). Fast and sensitive GCaMP calcium indicators for imaging neural populations. Nature *615*, 884-891. 10.1038/s41586-023-05828-9.
78. Sutter, M.L., and Loftus, W.C. (2003). Excitatory and inhibitory intensity tuning in auditory cortex: evidence for multiple inhibitory mechanisms. J Neurophysiol *90*, 2629-2647. 10.1152/jn.00722.2002.
79. Wehr, M., and Zador, A.M. (2003). Balanced inhibition underlies tuning and sharpens spike timing in auditory cortex. Nature *426*, 442-446. 10.1038/nature02116.
80. Polley, D.B., Read, H.L., Storace, D.A., and Merzenich, M.M. (2007). Multiparametric auditory receptive field organization across five cortical fields in the albino rat. J Neurophysiol *97*, 3621-3638. 10.1152/jn.01298.2006.
81. Higgins, N.C., Storace, D.A., Escabi, M.A., and Read, H.L. (2010). Specialization of binaural responses in ventral auditory cortices. J Neurosci *30*, 14522-14532. 10.1523/jneurosci.2561-10.2010.
82. Polley, D.B., Heiser, M.A., Blake, D.T., Schreiner, C.E., and Merzenich, M.M. (2004). Associative learning shapes the neural code for stimulus magnitude in primary auditory cortex. Proc Natl Acad Sci U S A *101*, 16351-16356. 10.1073/pnas.0407586101.
83. Polley, D.B., Steinberg, E.E., and Merzenich, M.M. (2006). Perceptual learning directs auditory cortical map reorganization through top-down influences. J Neurosci *26*, 4970-4982. 10.1523/JNEUROSCI.3771-05.2006.
84. Watkins, P.V., and Barbour, D.L. (2008). Specialized neuronal adaptation for preserving input sensitivity. Nat Neurosci *11*, 1259-1261. 10.1038/nn.2201.

85. Burton, S.D., Brown, A., Eiting, T.P., Youngstrom, I.A., Rust, T.C., Schmuker, M., and Wachowiak, M. (2022). Mapping odorant sensitivities reveals a sparse but structured representation of olfactory chemical space by sensory input to the mouse olfactory bulb. Elife *11*. 10.7554/eLife.80470.
86. Braubach, O., Tombaz, T., Geiller, T., Homma, R., Bozza, T., Cohen, L.B., and Choi, Y. (2018). Sparsened neuronal activity in an optogenetically activated olfactory glomerulus. Sci Rep *8*, 14955. 10.1038/s41598-018-33021-w.
87. Smear, M., Resulaj, A., Zhang, J., Bozza, T., and Rinberg, D. (2013). Multiple perceptible signals from a single olfactory glomerulus. Nat Neurosci *16*, 1687-1691. 10.1038/nn.3519.
88. Shusterman, R., Smear, M.C., Koulakov, A.A., and Rinberg, D. (2011). Precise olfactory responses tile the sniff cycle. Nat Neurosci *14*, 1039-1044. 10.1038/nn.2877.
89. Smear, M., Shusterman, R., O'Connor, R., Bozza, T., and Rinberg, D. (2011). Perception of sniff phase in mouse olfaction. Nature *479*, 397-400. 10.1038/nature10521.
90. Chong, E., Moroni, M., Wilson, C., Shoham, S., Panzeri, S., and Rinbert, D. (2019). Manipulating synthetic optogenetic odors reveals the coding logic of olfactory perception. BioRXiv.
91. Ackels, T., Erskine, A., Dasgupta, D., Marin, A.C., Warner, T.P.A., Tootoonian, S., Fukunaga, I., Harris, J.J., and Schaefer, A.T. (2021). Fast odour dynamics are encoded in the olfactory system and guide behaviour. Nature *593*, 558-563. 10.1038/s41586-021-03514-2.
92. Wilson, C.D., Serrano, G.O., Koulakov, A.A., and Rinberg, D. (2017). A primacy code for odor identity. Nat Commun *8*, 1477. 10.1038/s41467-017-01432-4.

Supplementary Figures.

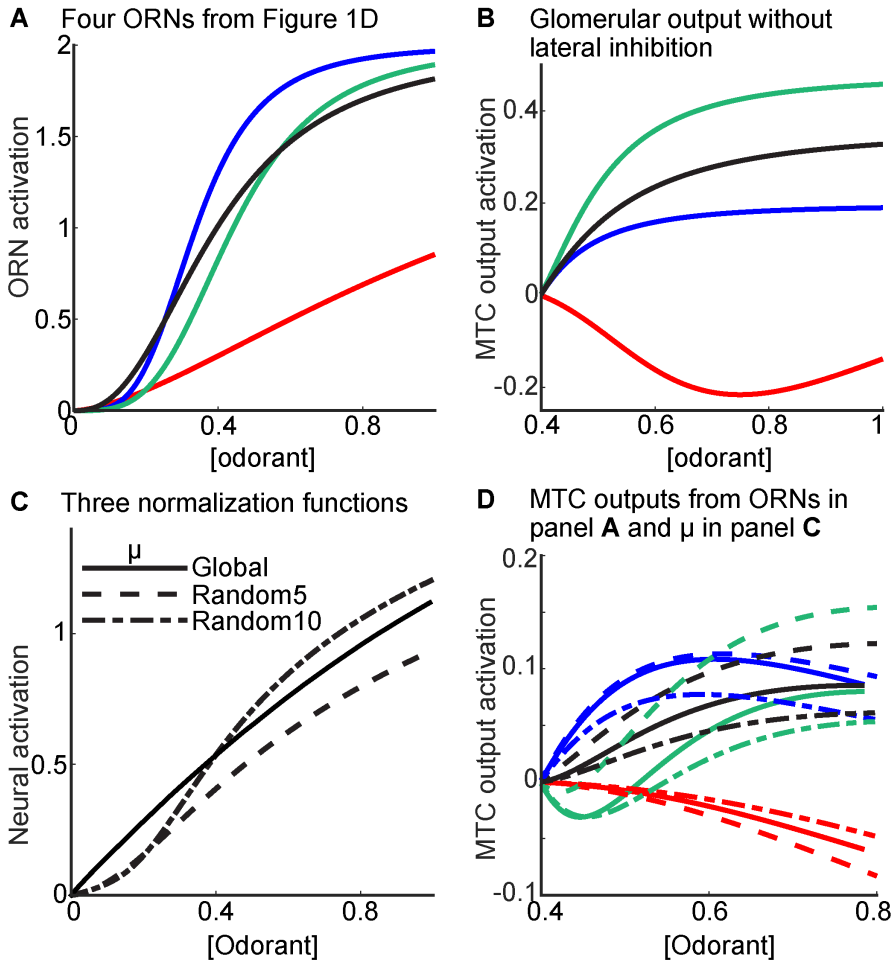

Supplementary Figure S1: (**A**) Four exemplar ORN concentration-response functions. To facilitate direct comparison, these signals are identical to those displayed in **Figure 1D**. (**B**) The four inputs from panel A have been processed by the local inhibition circuit (only) and the resulting MTC concentration-response functions (three I's and one DI). Importantly, no ID signals were generated in the absence of lateral inhibition. (**C**) Three different ORN normalization functions used to implemental lateral inhibition. The solid "μglobal" distribution is identical to the black dashed line in **Figure 1C**. Randomly sampling and then averaging 5 and 10 signals from that figure's ORN population yielded the "μRandom5" and "μRandom10" distributions, respectively (different dashed lines). (**D**) The four inputs from panel A processed using local inhibition and lateral inhibition implemented via the different normalization functions in panel **C**. All four MTC categories were present irrespective of which normalizing function was selected.

A jGCaMP8m

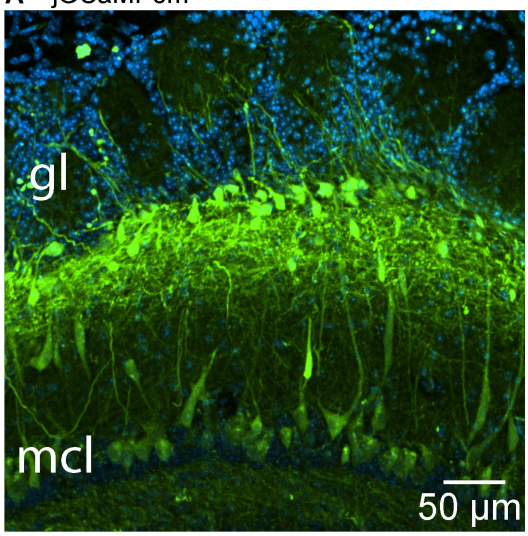

Supplementary Figure S2: (**A**) Histology from the olfactory bulb of a cross between the Tbx21-Cre and the TIGRE2-jGCaMP8m transgenic lines illustrating jGCaMP8m expression in mitral/tufted cells. gl, glomerular layer; mcl, mitral cell layer.

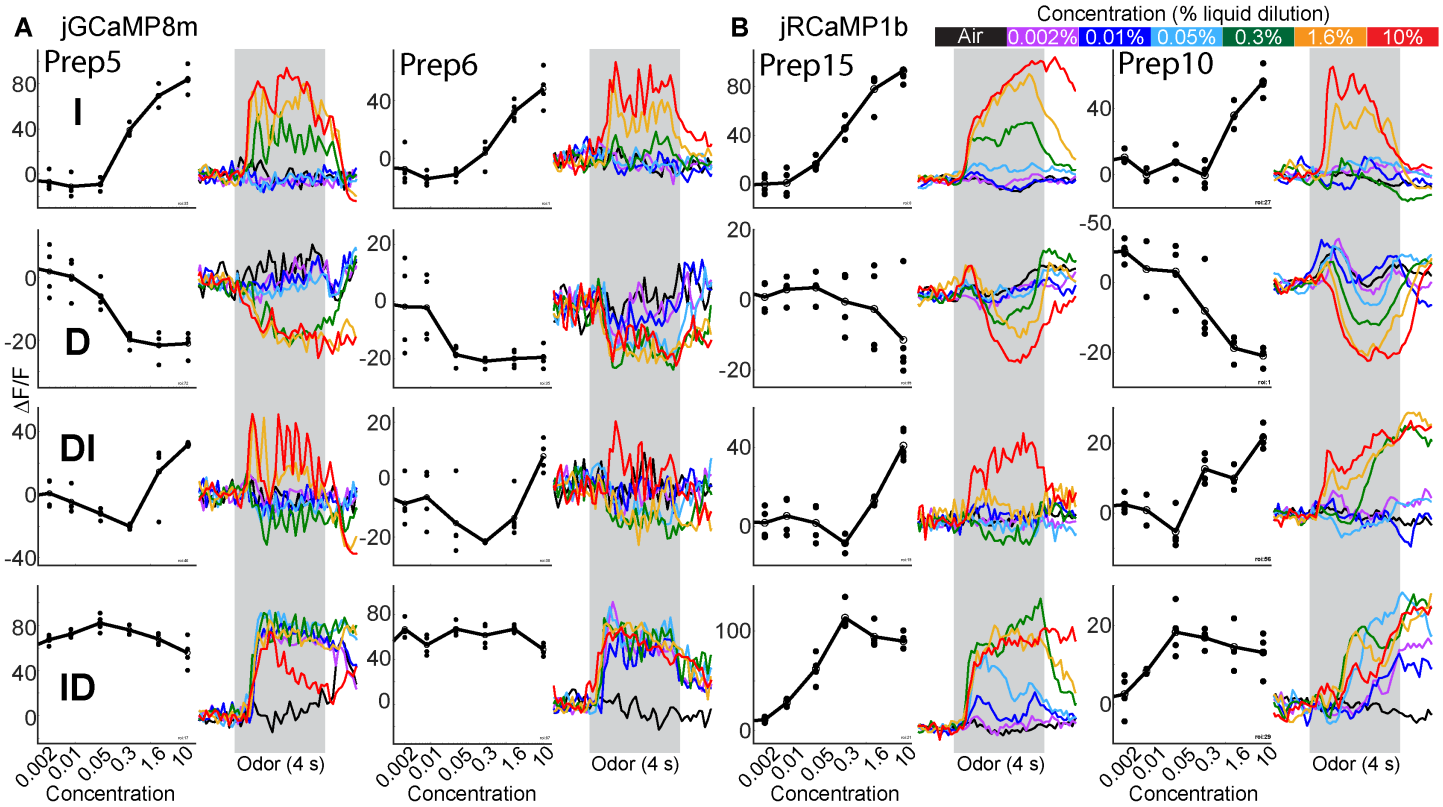

Supplementary Figure S3: MTC glomerular responses with increasing, decreasing, decreasing-increasing and increasing-decreasing response categories measured with jGCaMP8m (**A**) and jRCaMP1b (**B**).

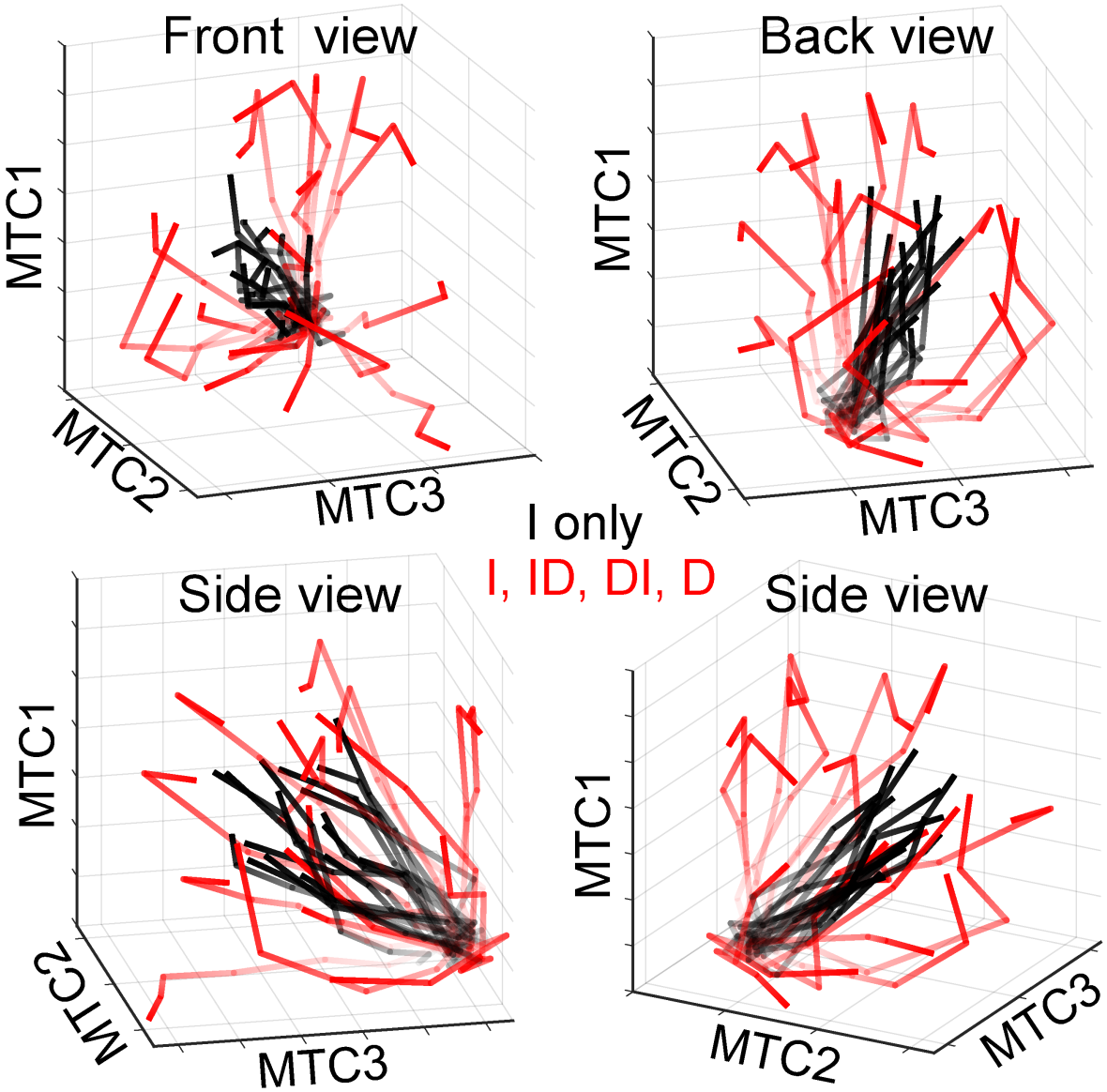

Supplementary Figure S4: Proposed model of how the non-canonical response types influence odor coding. Each line in this model illustrates the response of 3 MTC glomeruli to a single odor across concentration changes. Concentration changes are represented as the changing transparency of each line. MTC glomeruli with only increasing responses tended to cluster together in perceptual space (black lines). In contrast, MTC glomeruli with different response categories had response trajectories that diverged from one another. Each panel illustrates the projections from a different angle.